Final

AN EXPERIMENTAL STUDY OF THE FLOW FIELD ASSOCIATED WITH A JET ISSUING FROM A LIFTING WING IN CROSSFLOW

Howard M. McMahon* and D. L. Antani**

SUMMARY

An experimental program was conducted to determine the behavior of a round turbulent jet issuing from a lifting two-dimensional wing in crossflow. The jet was located at 65% wing chord on an NACA 0021 airfoil fitted with a 30% chord NACA 4415 flap. Surface pressures and forces on the model were measured at lift coefficients of 0.034, 1.24, and 2.45 with the jet off and with jet effective velocity ratios (square root of the ratio of the jet dynamic pressure to the freestream dynamic pressure) of 4, 6, and 8. Interference surface pressure distributions and interference lift are compared with previous results for the wing alone.

The flow field associated with the jet was surveyed extensively with directional pressure probes to determine local velocity vectors as well as pressures for the same values of the test parameters. Data describing the jet centerline and the path of the contrarotating vortices accompanying the deflected jet are presented and compared with similar data for a round jet issuing from a large flat plate. The spacing and strength of the vortices are calculated using a simple vortex model previously proposed for the flat plate case.

The results show that the penetration of the jet and the vortices increase significantly with increasing lift for the range of test parameters covered in the study. The calculated vortex spacing and strength also show an increase with lift.

---

* Professor of Aerospace Engineering, Georgia Institute of Technology, Atlanta, Georgia.

** Assistant Research Engineer, Aerospace Engineering, Georgia Institute of Technology, Atlanta, Georgia.

INTRODUCTION

One of the critical flight regimes of a VTOL aircraft is during the transition from vertical to horizontal flight. During this transition, when the weight of the vehicle is being transferred from the thrust of the lifting jet to the lift on the wings, the vehicle suffers lift loss and pitching moment changes which are caused by a complex interaction between the downward-directed jet flow and the freestream flow. References 1 and 2 give a good summary of this aerodynamic interaction problem.

This problem has received attention from many investigators. Several experiments (for example, refs. 3, 4, and 5) have been conducted with a jet (usually circular) issuing from a large flat plate into a crossflow, with emphasis on the penetration of the jet and the pressure distribution on the flat plate. Theories (for example, ref. 6) have been developed to predict these phenomena. More recently, attention has turned to measurements in the wake between the jet plume and the flat plate (for example, refs. 7 and 8) and to studies of the two large contrarotating vortices which are a dominant feature of the flow field around the jet (ref. 9). Fearn and Weston (ref. 10) have made a complete mapping of the velocity field in and around the jet issuing from a large flat plate, and the results have been used in two different analytical models for predicting the strength of the vortices.

The flat plate case retains the essential flow features of the interaction problem while eliminating complications such as pressure gradients and the presence of circulation and trailing vortices which would be present in the problem of a jet issuing from a finite wing. The jet issuing from a wing into a deflecting stream has not received nearly the detailed study as has the flat plate case. Surface pressure and force measurements on finite wings in the presence of deflected jets have been reported in references 11 and 12. Mikolowsky (ref. 13) measured surface pressures and forces on a two-dimensional wing with a "clean" configuration, that is, the jet plenum chamber was supplied by air piped internally in the wing.

The purpose of the present work is to extend the work of Fearn and Weston (ref. 10) to a mapping of the velocity field in and around a jet in the presence of circulation, that is, a jet issuing from a lifting two-dimensional wing. The experimental study combines the experimental configuration used by Mikolowsky (ref. 13) with the measurement techniques developed by Fearn and Weston (ref. 10). The objective is to compare data from the wing tests with those from the flat plate in order to investigate changes in the velocity field and the vortex strength and location brought about by the presence of the lifting wing. The data should also be useful in helping to formulate analytical models of the wing-jet interaction.

SYMBOLS

The units of measure used in this report are given in both the International System of Units (SI) and, parenthetically, in the U. S. Customary Units.

c	wing chord
c_f	flap chord
C_L	lift coefficient based on wing area
C_p	pressure coefficient, $\frac{p - p_\infty}{q_\infty}$
C_{p_o}	stagnation pressure coefficient, $\frac{p_o - p_{o_\infty}}{q_\infty}$
d_j	jet exit diameter
D	drag force
h	half-spacing of vortices
L	lift force
p	pressure
p_o	stagnation pressure
PM	pitching moment about half-chord of wing
q	dynamic pressure
Re	Reynolds number
T	jet thrust
$\overline{T}$	temperature
U_v, V_v, W_v	velocity components in the vortex cordinate system
V	velocity
x	chordwise distance from leading edge of wing or flap

X,Y,Z	cartesian wind tunnel coordinate system (see fig. 10)
X_v, Y_v, Z_v	cartesian vortex coordinate system (see fig. 10)
X_o, Z_o	location of middle probe of rake at the start of a traverse (wind tunnel coordinate system)
α	wing angle of attack
Γ	strength of a vortex filament
γ	$\frac{\Gamma}{2d_j V_\infty}$
δ	flap deflection angle, positive when deflected down
ϵ	rake pitch angle measured from Z axis, positive clockwise
λ	effective velocity ratio, $\lambda^2 = \frac{\rho_j V_j^2}{\rho_\infty V_\infty^2}$
ρ	density
ΔC_p	interference pressure coefficient (jet-on C_p minus jet-off C_p)
$\frac{\Delta D}{T}$	interference drag coefficient (jet-on D minus jet-off D divided by jet thrust)
$\frac{\Delta L}{T}$	interference lift coefficient (jet-on L minus jet-off L divided by jet thrust)
$\frac{\Delta PM}{Td_j}$	interference pitching moment coefficient about half-chord of wing (jet-on PM minus jet-off PM divided by Td_j)
ΔX, ΔZ	incremental distance between data points in wind tunnel coordinate system

Subscripts:

a	ambient
B	wind tunnel balance readout
C	wind tunnel balance calibrated value
j	jet exit plane
p	plenum chamber
∞	freestream conditions

EQUIPMENT AND INSTRUMENTATION

The basic wind tunnel model and some of the support equipment and calibration procedures were identical with those used by Mikolowsky (ref. 13). Only a brief summary of those items common to both experiments will be presented here; the reader is referred to reference 13 for a detailed discussion.

Wind Tunnel

The experiments were conducted in the Georgia Tech 2.74 meter (9.0 ft) wind tunnel, which is a closed return atmospheric type tunnel having a circular test section. The tunnel turbulence factor is 1.2. In order to provide two-dimensional flow around the wing model, the circular test section was modified by installing flat sidewalls, which gave a model span of 2.18 m (7.17 ft). A drawing of the modified test section, with the model and rake actuator installed, is given in figure 1. The fairing on the floor of the test section covers a pitch strut which is attached to the wind tunnel balance and which could not be removed for these tests. Photographs of the test section are shown in figure 2.

Wing and Flap

The two-dimensional wing model had an NACA 0021 airfoil section modified such that it had a straight-line contour from the 80% chord station to the trailing edge. The model had a chord of 39.04 cm (15.37 in.) and was fitted with a transition strip 9.65 mm (0.38 in.) wide centered at 5% chord on both the upper and lower surfaces. The wing was instrumented with 191 surface pressure taps whose location is tabulated in reference 13. The pressure taps were arranged so as to give detailed coverage on the lower surface near the jet exit and lesser coverage on the upper surface. There were sufficient taps in

the spanwise direction to check on the two-dimensionality of the flow with the jet off.

In the tests of reference 13, the wing exhibited incipient stall at $\alpha = 9^{\circ}$ at a lift coefficient of 0.80. Since the motivation for the present tests was to determine the behavior of the deflected jet in the presence of circulation, a flap was fitted to the model in order to increase the maximum lift coefficient. The flap had an NACA 4415 section with a chord of 11.71 cm (4.61 in.), that is, 30% of wing chord, and was made from laminated mahogany (fig. 3). Cost and available machining capability prevented the flap from being made of metal. The flap was fabricated by cutting airfoil sections from 1.59 cm (0.625 in.) mahogany plank and mounting the sections side-by-side on two stainless steel tubes (fig. 4). Four sections were machined from 1.59 cm (0.625 in.) aluminum plate and each of these four sections was drilled to accomodate surface pressure taps in the flap, arranged in 2 chordwise rows on the upper surface (7 taps each row) and 4 chordwise rows on the lower surface (7 taps each row). These aluminum sections were placed between appropriate mahogany sections such that the chordwise pressure taps in the flap were aligned with existing chordwise taps in the wing at span locations $Y/d_j = 0$, 0.69, 1.37, and 2.07. Table 1 gives the precise location of the pressure taps on the flap. The two stainless steel tubes inside the flap provided rigidity and alignment, gave a solid attachment point for the flap mounting brackets, and allowed the vinyl tubing from the pressure orifices to be led from the central portions of the flap to the tunnel sidewalls. Upon final assembly, the individual airfoil sections were bonded together and the flap was mounted in a lathe where the precise contouring of the mahogany section was achieved by running a small high speed grinder in the spanwise direction between two templates. The wood then was sealed and finished with lacquer.

The flap was attached to the wing at four points located 38.1 cm (15 in.) and 99.1 cm (39 in.) on either side of the wing centerline. These locations corresponded to 10 and 26 jet diameters. The attachment brackets allowed for continous adjustment of flap deflection angle by rotation of the flap about its leading edge. The flap leading edge location was fixed at 0.10% of wing chord behind the wing trailing edge and 4.5% of wing chord below the wing trailing edge. This leading edge location was suggested by NASA Langley Research Center based upon computer optimization studies for maximum lift coefficient with this wing-flap combination.

The jet exit in the wing was 3.81 cm (1.5 in.) in diameter and was located on the wing centerline at the 65% wing chord location. The jet nozzle consisted of a simple bellmouth with a straight extension leading from the plenum chamber inside the wing to the model surface. The exit extension was flush with the wing countour and the nozzle/wing panel interface was sealed with dental dam. The jet flow at the exit was normal to the wing chord. The quality of the turbulent jet outflow as regards uniformity across the exit area and length of the jet core in still air had been determined in the tests reported in reference 13 and these tests were not repeated here.

Rake

The velocity in and around the deflected jet was measured with the same rake of seven yaw-pitch probes which had been used in previous experiments by Fearn and Weston (ref. 10). Each probe has a hemispherical tip and was 6.35 mm (0.25 in.) in diameter and 20.32 cm (8 in.) long, with a 5.08 cm (2 in.) spacing between probes. To measure the yaw and pitch angles there were 4 pressure ports, placed at approximately 45° to the total pressure port, in the directions of yaw and pitch. Each probe had a ring of 7 interconnected static ports located 5.08 cm (2 in.) from the tip. Data taken at NASA Langley Research Center subsequent to the experiments reported in reference 10 indicated that it was preferable to calculate static pressure from the measured total, pitch, and yaw pressures than to measure it directly. Hence the data reduction program was modified accordingly, and it was this modified program that was used for the tests reported here. The rake is shown in figure 5.

As a check on the program and on the condition of the rake, the rake was mounted on a single support in the empty wind tunnel test section and set at known angles of yaw or combined pitch and yaw. The five pressures measured for each probe under evaluation were then used as inputs to the data reduction program. The test results indicated an error in yaw angle of less than 1° up to angles of 30°. At 15° pitch, and with yaw angles up to 30°, the free-stream velocity calculated from the pressure readings was within 1% of that measured independently in the test section. With the rake pitched 15°, the measured velocity component parallel to the probe axis (U_v) was within 2% of the correct value. On the basis of these tests it was concluded that the rake was behaving satisfactorily. The computer program supplied with the rake was used without modification, except to incorporate the minor change that the rake was to be used here with a jet directed downward whereas the program had been written for a jet directed upward from a flat plate.

The probe spacing on the rake was 5.08 cm (2 in.) while the jet diameter was 3.81 cm (1.5 in.). In order that the data would be spaced in even multiples of the jet diameter, only two of the seven probes (one end probe and the middle probe of the rake), spaced 4 jet diameters apart, were used for the calibration runs and for taking data. The probe at the opposite end of the rake previously had been shown to be defective. (The probes used in these tests were numbered 4 and 7). The rake was oriented with the probes arranged vertically and with the active probe on the top. Since the time required to measure the probe pressures was much longer than that required to move the rake, the use of only two probes of the seven did not seriously hamper the data-taking.

Actuator

In order to take the required data it was necessary that the rake be translated in three dimensions in the region downstream of the jet exit. It was also necessary that the rake be rotated so that the probes were at least approximately aligned with the jet flow, since at large flow angularities the

uncertainty in measured flow direction becomes large. An existing actuator was rebuilt to meet these requirements.

The horizontal lead-screw drive of the existing actuator (component 1 in fig. 6) was attached to the ceiling of the test section as far downstream as possible, and the drive motor was replaced with a stepping motor. A new vertical drive (component 2) was fabricated using two guide rods each 2.54 cm (1.0 in.) in diameter with a lead-screw and stepping motor. A traveling rake-holder contained internal gearing and a stepping motor so that the 2.54 cm (1.0 in.) diameter side-support tube for the rake could be rotated about its axis in order to pitch the rake. This rake-holder is shown in figure 5. The bottom of the vertical drive assembly contained a spring-loaded fitting which rode on an axial guide rod bolted to the tunnel floor. Care was taken that the actuator be made as rigid as possible.

The actuator vertical drive was mounted 45.7 cm (18 in.) or 12 jet diameters to one side of the wing centerline. The rake-holder could be moved in a streamwise direction from the flap trailing edge to 35 jet diameters downstream, and from 4 jet diameters above the wing to 21 diameters below it. These two translatory motions of the actuator, as well as the rotation of the rake, could be manually or computer controlled. The spanwise location of the rake was set manually by sliding the rake side-support tube in the rake-holder and locking it in place.

In order to limit rake travel for safety reasons, small moveable limit blocks fitted with microswitches were placed at the top and bottom of one vertical guide rod and on the upstream and downstream end of one horizontal guide rod of the actuator. The lower and downstream microswitches additionally provided a zero reference to which the rake-holder could be returned at any time during a test run in order to check the known rake location against that shown on the read-out display.

The downstream end of the rake axial support tube was fitted with a precision mercury switch carefully aligned so as to be parallel with the shank of the rake. When the rake was moved spanwise it was necessary to unlock the side-support tube in the rake-holder and the zero reference for rake pitch was lost. This switch allowed the zero to be re-established quickly and accurately using the rotation stepping motor under manual control.

Relay contact closures in the computer provided pulse inputs to three motor controllers which in turn drove the three stepping motors. The limit switches and mercury switch were so arranged in the circuit that when they were closed this interrupted the drive signal from the computer to the motor controller and the motors were stopped.

An up-down counter was incorporated in the circuit between each motor controller and stepping motor. These instruments counted the pulses sent to the stepping motors and hence gave a visual display of rake position and pitch

angle. There remained the possibility that a stepping motor might received a pulse and then slip, hence the use of the limit switches as zero reference checks. The resolution of the counters was 0.025 mm (0.001 in.) in X, 0.127 mm (0.005 in.) in Z, and one minute of arc.

The wind tunnel console and the rack containing the stepping motor controls and up-down counters are shown in figure 7.

Force Measurement System

The wind tunnel is equipped with a six-component yoke balance which was used to simultaneously record wing lift, drag, and pitching moment. The forces and moments were displayed on counters and recorded on a printer.

The two-dimensional model was mounted ten inches above the tunnel centerline, with the ends supported on pylons which are part of the balance system. Circular endplates, aligned flush with the sidewall, were fitted to the ends of the wing. Where these endplates mated with the sidewall there was a small annular channel. Thus the wing was "floating" on the balance system. It was originally intended that the annular channel would contain an inflatable seal. However, earlier tests (ref. 13) had shown that the seal, even when deflated, introduced extraneous non-repeatable forces into the balance system by acting as a connection between the wing and the wind tunnel structure. The seal was not used in the present tests, with negligible effect on force and pressure measurements. The flap lay outside of the area covered by the end plates, so it was made such that there was a small clearance between the end of the flap and the sidewall structure.

The plenum chamber was fitted inside the wing in such a way that it was isolated from the wing structure. The chamber was supported by four flexures, each flexure being fitted top and bottom with a double strain gage wired as a four-arm bridge. A regulated power supply provided 5.0 volts excitation to each bridge. The output of each bridge was led to a D. C. amplifier and the amplifier signals were read through an integrating digital voltmeter by means of a scanner controlled by a computer. Suitable calibration of these strain gages allowed a direct measurement of the jet thrust.

Air Supply

Ideally, the model should be supported only by the balance system and be free of any connections which might ground the system to the wind tunnel structure. Since air had to be supplied to the model, this ideal could not be met but care was taken to minimize the effect.

The jet air was furnished by a 7.46×10^4 N.m/sec (100 hp) centrifugal compressor which supplied a maximum discharge pressure of 5.52×10^4 N/m^2 (9 psi).

The supply air was led through a 15.24 cm (6 in.) inside diameter pipe to a tee and thence through two trapeze arrangements (fig. 8), installed symmetrically on either side of the test section, and into the wing. This arrangement of metal pipe and rubber hoses was designed to minimize interference with the balance readings due to pressurization of the supply lines and/or flow through the lines, as well as providing good balance zero returns. The system was patterned after the air supply installation at the Lockheed Georgia Company wind tunnel.

Pressure Measurement System

The freestream total pressure was taken from a probe mounted on the ceiling of the test section, while the test section static pressure was taken from a wall pressure tap installed 50 cm (19.7 in.) upstream of the wing leading edge. These pressures, as well as the plenum chamber stagnation pressure, the wing and flap surface pressures, and the rake pressures, were measured using variable-capacitance transducers. These transducers responded to differential pressure, with one side being open to ambient pressure.

The transducer used to measure plenum chamber pressure had a maximum range of 5.17×10^4 N/m^2 (7.5 psi). The output of the signal conditioner (10 V full scale) was monitored on a digital voltmeter.

The transducers used to measure surface and rake pressures had a maximum range of 1000 mm Hg. For surface pressure measurements the signal conditioners were set manually at a fixed range scale of X 0.03 (full scale 30 mm Hg., output 10 V). The signal conditioner output was read by a computer through a scanner and an integrating digital voltmeter having an adjustable integrating time. The rake pressures were measured with signal conditioners which could be set manually over a 3 decade range or set at range scales of X 1.0, X 0.1, and X 0.01 (with 10 V full scale output) under computer control through a suitable contact closure. The output of these signal conditioners was read by a computer through a crossbar scanner and an integrating digital voltmeter with a 1/60 sec integrating time. The data from the computer were stored either on paper tape (surface pressures) or disc (rake pressures). All of the signal conditioners provided an identification voltage output, the value indicating which range scale had been set. Figure 9 shows the data acquisition system for the rake pressures.

The wind tunnel freestream dynamic pressure was determined from measurement using calibrated piezometer rings. The pressure was monitored on a water manometer during a test run.

The wing and flap pressure tubing was led to pressure sampling scanners mounted on the wing endplates so as to minimize the number of connections between the wind tunnel balance and the tunnel structure. The tubing from the rake was led to a pressure scanner mounted just outside the test section at the midpoint of the horizontal and vertical travel limits of the actuator.

A typical rake probe tubulation contained 20.3 mm (8 in.) of 0.81 mm (0.032 in.) inside diameter stainless steel tubing, 25.4 cm (10 in.) of 1.07 mm (0.042 in.) I.D. vinyl tubing, and approximately 2.74 m (9 ft) of 1.60 mm (0.063 in.) I.D. vinyl between the pressure orifice and the pressure scanner. All pressure scanners were actuated by solenoids which could be under manual or computer control.

TESTING PROCEDURES AND CONDITIONS

The axis system and nomenclature used in the tests are shown in figure 10. The X,Y,Z wind tunnel coordinate system has its origin at the jet exit on the airfoil surface and not at the wing chordline. Note that the origin moves with wing angle of attack. The X_v, Y_v, Z_v coordinate system has its origin along the vortex curve, with the Y_v-Z_v plane being perpendicular to the vortex curve.

Wind Tunnel Flow

All of the experiments were conducted at an indicated freestream velocity of 30.48 m/s (100 ft/sec), which corresponds to a Reynolds number (based on wing chord) of 8.15×10^5. The wind tunnel was operated at a constant value of freestream dynamic pressure corresponding to this indicated velocity at standard conditions. However, the data were always nondimensionalized with the measured freestream quantity appropriate to the test in question. The dynamic pressure varied ± 2% over the course of the various tests. Prior to installation of the wing model, a dynamic pressure survey of the test section was made from wall to wall in the plane of the wing chordline and approximately at the mid-chord location. The freestream velocity was found to be constant across the test section to within ± 1% except for about 10.16 cm (4.0 in.) next to the sidewalls where the boundary layer was present. The survey probe was then set at the tunnel centerline and the water manometer, which was used by the operator to set freestream conditions, was calibrated.

Wing-Flap Configuration

Data were taken for three combinations of wing angle of attack and flap deflection angle: $\alpha = 0^\circ$, $\delta = -5^\circ$ (minimum lift); $\alpha = 6^\circ$, $\delta = 0^\circ$ (intermediate lift); and $\alpha = 8^\circ$, $\delta = 15^\circ$ (maximum lift). The wing angle of attack was adjusted manually by aligning holes in an incidence bar mounted on the air supply pipe in the wing with holes in an incidence plate rigidly fastened to the balance pylon. The flap angle was set with a template and inclinometer. The flap deflection angle was measured to be constant within $\pm 0.5^\circ$ over a spanwise region 91.44 cm (36 in.) on either side of the wing centerline. Outboard of this region, within about 15.24 cm (6 in.) from the tunnel sidewall, the flap deflection angle increased by 0.75 - 1.0° because of warpage in the flap. Once set, the flap deflection angle did not change

during a test run and a specified flap angle setting was repeatable within ± 0.5 degrees.

The minimum lift configuration of $\alpha = 0^\circ$, $\delta = -5^\circ$, was found by setting the wing at zero angle of attack with the jet off and varying the flap deflection angle until the lift was essentially zero ($C_L = 0.034$).

The lift optimization studies run on the computer at NASA Langley Research Center had indicated that, with this wing-flap combination at this Reynolds number, the wing-flap spacing specified should yield a lift coefficient maximum value of $C_L = 3.55$ (based on wing chord) with $\alpha = 8^\circ$, $\delta = 30^\circ$. When this setting was tried it was observed from tufts that the flow was separating over the entire upper surface of the flap. This observation was confirmed by measuring flap surface pressures chordwise along the flap centerline. The same behavior was observed at $\alpha = 8^\circ$, $\delta = 20^\circ$. At $\alpha = 8^\circ$, $\delta = 15^\circ$, the surface pressures showed no separation on the upper surface of either the wing or the flap. Flow visualization with oil flow on the flap upper surface indicated a separation bubble between 20% and 30% of flap chord, followed by attached flow to the flap trailing edge. This was considered to be acceptable, and the maximum value of C_L which was achieved with this configuration was $C_L = 2.45$.

The intermediate lift case was chosen to be about one-half of the maximum lift, and was attained with a convenient combination of $\alpha = 6^\circ$, $\delta = 0^\circ$.

Jet

The effective velocity ratio of the jet, λ, is defined as

$$\lambda^2 = \frac{\rho_j V_j^2}{\rho_\infty V_\infty^2} = \frac{q_j}{q_\infty} .$$

For each of the three lift cases, data were taken at $\lambda = 4$, 6, and 8. Surface pressures and wing forces and moments were also measured at $\lambda = 0$ to serve as references against which to evaluate the interference effect of the jet flow.

After the tunnel had been brought up to speed, q_∞ was calculated using the measured test section static pressure and total pressure. The required value of λ then specified the value of q_j which was needed. From this value of q_j the required plenum stagnation pressure was calculated using

$$p_{o_p} = p_\infty + (1.01)\, q_j$$

where the factor 1.01 was obtained from previous calibration of the losses in the nozzle when run as a free jet. The jet plenum total pressure was monitored on a digital voltimeter and held within ± 1.0% of reading. Because the jet air was heated by compression in the blower, the plenum stagnation temperature was between 49°C (120°F) and 71°C (160°F). This temperature was monitored on a thermocouple read-out and the desired plenum pressure was set only after the stagnation temperature had reached an equilibrium value.

The character of the outflow from the nozzle at the 65% wing chord station had been investigated previously (ref. 13) by running the nozzle (with the same plenum chamber and air supply system) in a large room as a free jet. The velocity profiles measured along two diameters in the exit plane were constant with ± 1.7% over the central 85% of the exit diameter. The core of the jet was measured along the centerline and found to be two diameters long.

Force Measurements

Two different types of force measurements were made. One involved measuring model lift, drag, and pitching moment with the wind tunnel balance while the other was a direct measurement of jet thrust using strain gages. Each will be described briefly.

The wind tunnel balance was calibrated by loading the model statically in the negative lift direction on the wing trunion axis (balance centerline), in the positive drag direction in the plane of the wing chordline, and in positive pitch by applying known loads in the lift direction at a point one foot aft of the trunion axis. Since the model was mounted above the balance centerline, there was a significant interaction of drag into pitching moment. Other interactions were negligible. A least squares straight line fit to the calibration data led to the following results:

$$L_C = 0.997\ L_B$$

$$D_C = 0.998\ D_B$$

$$PM_C = 1.005\ PM_B - 0.824\ D_C$$

These calibration constants were almost identical with those determined in reference 13. For these calibrations the air supply hoses and all necessary wiring and tubing were connected to the model but there was no seal between the wing endplates and the tunnel sidewall. During two runs with the jet off, the resulting small annular gap was covered with dental dam. Sealing the gap resulted in a less than 1% change in measured lift at the maximum lift condition, so all subsequent data were taken with the seal removed.

It was necessary to determine the balance tares resulting from pressurization of the air supply hoses and momentum flux caused by air flow in the supply piping. The tares in lift and drag from both of these causes were found to be negligible (i.e. within the zero return of the balance). However, there was a tare in pitching moment at the higher supply pressures and mass flows which could not be eliminated in the time available.

The wind tunnel balance zero returns were determined as ± 0.89 N (0.2 lb) in lift and drag and ± 0.27 N.m (0.2 ft-lb) in pitching moment. For the minimum lift case with the jet off, the lift and drag were repeatable within ± 3% and the pitching moment within ± 7%. At higher values of lift the repeatability was better percentage-wise except for the intermediate lift case where the pitching moment was very small.

The normal force on the plenum chamber, i.e. the jet thrust, was measured using strain gages mounted on the flexures which supported the chamber inside the wing. This internal balance had been calibrated previously (ref. 13) and the calibration constants were verified by loading the plenum chamber along the centerline of the jet exit and in the thrust direction. The calculated thrust agreed with the applied value within one percent. These checks were repeated with a dental dam cemented between the jet exit-wing panel interface, as would be the case during a wind tunnel run. The linear relation between applied and measured thrust changed slope by 5%, and the measured jet thrust during wind tunnel runs was corrected for this effect. The strain gage signals were read by taking the average of ten readings from a digital voltmeter set to integrate each reading over one second. Jet thrust levels were between about 15.57 N (3.5 lb) and 75.61 N (17 lb), with the accuracy of the measurement estimated to be ± 2.0%.

The major source of error in the interference force measurements was the wind tunnel balance system, since the differences between the jet-on and jet-off values were small. Except for the minimum lift case, the values of $\Delta L/T$ are estimated to be accurate within ± 10%. However, the drag differences were so small that the data should be interpreted as showing trends only, and the same should be said for the values of $\Delta PM/Td_j$ because of the additional factors of repeatability of the pressure and momentum tares and the interaction of drag into moment.

Pressure Measurements

As has been noted earlier, all pressures were measured with variable capacitance transducers. These transducers were calibrated with a dead-weight tester over the range of pressures (i.e. range scale settings) for their particular application. All of the transducers exhibited linear calibration curves with slopes differing from unity by less than one percent.

Surface pressures. - The surface pressures on the wing and flap were acquired using essentially the same computer program as was used in reference 13. The output of the transducer signal conditioners was measured with an integrating digital voltmeter set at 0.1 seconds, and an average of ten such readings was taken for each data point. Measured values of q_∞ and p_∞ were recorded during a run for later data reduction to pressure coefficient form.

The first test runs were used to determine the jet-off pressure distribution, and interference pressure coefficients defined as

$$\Delta C_p = C_{p_{jet\text{-}on}} - C_{p_{jet\text{-}off}}$$

were obtained from jet-on pressure distributions measured in subsequent runs. The pressure readings were observed to fluctuate about ± 2% of q_∞ in regions forward of and lateral to the jet and about ± 5% of q_∞ in the wake region aft of the jet. The data averaging helped to reduce errors due to these fluctuations, the repeatability in C_p measurements being within ± 2% except in the wake where it was ± 4%.

The wing pressures were output on paper tape and reduced to interference pressure coefficient form for later machine-plotting of constant pressure contours.

Rake pressures. - It was required to measure five pressures from each of the two active probes in the rake. In addition, the freestream total and static pressure was recorded at the start of every rake traverse. During many of the traverses there was an overlap in location between one probe and the other, and the repeatability in the calculated velocity components at these overlap points was satisfactory.

Each pressure tube from the rake was connected to a tee at the pressure scanner so that orifice 1 from one probe of the rake was connected to scanner ports 1 and 6, orifice 2 to ports 2 and 7, and so on. The five tubes from the other probe were connected to a second pressure scanner, with both pressure scanners being on a common drive (fig. 11).

The time lag in the rake pressure measurement system was estimated following the method of reference 14. It was concluded from these calculations that, for the tubing lengths used, a waiting time of less than one second after the rake had been moved to a new location would yield negligible time lag error in the measured pressure. In order to be conservative, a delay of 3 seconds was used after each rake movement before any pressures were measured, and a delay of 2.2 seconds was used after the step command to the pressure scanner before the pressure at the next scanner port was measured.

The acquisition of the rake pressure data will be described in a later section.

Rake Positioning

The actuator system was such that as the rake moved away from the wing centerline it came closer to the rake-holder and vertical guide rods. It was felt necessary to determine how close the rake could come to the rake-holder before interference effects from the actuator would render the rake data suspect. Accordingly, as part of the preliminary rake calibration, a dummy vertical actuator was constructed from aluminum tubing with a rake-holder made of wood, and this dummy actuator was installed in the empty test section. The rake was set on the tunnel centerline at $\alpha = 0^{\circ}$ and then moved progressively closer to the rake-holder while the changes in yaw angle and total velocity were determined. It was found that the variations in these quantities from their reference values on the centerline were less than one degree and one percent, respectively, up to a spanwise rake location of $Y/d_j = 10$. The furthest rake location from the centerline in the data tests was $Y/d_j = 5.5$.

The actuator was installed in the test section after the force and surface measurements had been taken. It was aligned in the streamwise direction by observing the rake travel in the X-direction with a transit. The vertical alignment was done by moving the rake in the Z-direction along a plumb line. The up-down counters, which gave a visual display of the rake location in X and Z as well as rake pitch angle, counted pulses sent by the motor controllers to the stepping motors in order to display information to the operator. Likewise, the computer kept track of rake position and angle by counting the contact closures which sent pulses to the motor controllers. There existed, then, the possibility that a pulse might be sent to the motor and counted whereas the rake did not move with that pulse because the stepping motor slipped. In order to determine the maximum pulse rate to the motors without slippage occurring, dial gages were set up at either end of a 10.2 cm (4 in.) travel in X and Z and the pulse rates were varied until the rake-holder would stop with an error of $\pm$ 0.050 mm (0.002 in.) over the interval. The pulse rate in rotation was adjusted such that the rake would return to zero with a repearability of $\pm 0.2^{\circ}$. This was the minimum repeatability attainable in pitch, and was attributed to oscillation of the mercury in the mercury switch. The pulse rates that were used corresponded to a rate of travel of the rake-holder of 4.83 mm/s (0.19 in./sec) in X, 3.81 mm/s (0.15 in./sec) in Z, and 0.60 degrees/sec in rotation. The zero-reference limit switches in X and Z had a repeatability of less than 0.035 mm (0.001 in.) and these switches were set at a known location by using the counters to measure distance. There was an option in the computer program such that after a desired number of traverses the rake would be returned to its reference zero (limit switch) position in Z. This option was used most often when the rake was near the wing. A log was kept of the variation of the counter reading from zero when the counter stopped due to activation of the limit switch. Typically, the discrepancy was less than $\pm$ 0.127 mm (0.005 in.). The pitch zero was checked manually whenever the

zero in Z was taken. The actuator took considerably longer to run back to the downstream limit switch, so that the zero reading in X was checked less frequently. Typically, it was in error by less than ± 0.25 mm (0.010 in.). Whenever any zero reading did not check satisfactorily (which happened rarely) the rake traverses were repeated.

The movement of the rake during a traverse constituted a series of changes in both X and Z. A log was kept of the initial and final counter readings for each traverse and these were checked against the correct values. The difference in X was less than ± 1.27 mm (0.050 in.) and in Z less than ± 0.13 mm (0.005 in.).

Considering all of the above factors, it was estimated that during the taking of data the rake position error in X was ± 1.27 mm (0.05 in.), in Z ± 0.25 mm (0.01 in.), and in the rake pitch angle ± 0.3°. The Y location of the rake was set manually using a steel scale, with an estimated position error of ± 1.27 mm (0.05 in.).

Although the axial drive component of the actuator was hung from the test section ceiling as far downstream as the wind tunnel structure would allow, there was some unavoidable aerodynamic interference between the actuator and the wing. In order to estimate this effect, lift forces for the minimum and intermediate lift cases were measured with the actuator installed and with the vertical drive in the downstream position. The actuator interference lift corresponded to a reduction in wing angle of attack of about 0.5°. Wing surface pressures were measured for the minimum lift case with the same actuator configuration. They confirmed this estimate, and also showed that the two-dimensionality of the flow had not been affected significantly.

Rake

The pair of contrarotating vortices in the deflected jet induces an upwash in the plane of symmetry (Y = 0). The locus of points with maximum induced upwash in the symmetry plane is a measure of the trajectory of the vortex pair. The projection of the vortex trajectories onto the symmetry plane is defined as the vortex curve, and it was desired to take data in planes perpendicular to these vortex curves. As a preliminary step, then, these planes had to be determined. Since there were no available data describing the vortex curve of a jet exhausting from a wing, the empirical vortex curve equation of Fearn and Weston (ref. 10) for the flat plate case was used to set up preliminary rake traverses in the plane of symmetry for the wing case. Preliminary traverses were made at five values of X/d_j for the zero and maximum lift cases with $\lambda = 4$ and $\lambda = 8$. These data were plotted as W_v versus Z_v and the locus of points of maximum upwash for each condition was used to determine approximate vortex curves for the jet issuing from the wing. These curves in turn were used to define the appropriate angles for the traverses used in the data runs. Since the vortex curves found from the data runs

were not greatly different from those used to set up the traverses for the data runs, it was judged to be unnecessary to make a second iteration on the vortex curves. The traverse angles for $\lambda = 6$ and for the intermediate lift case were determined by interpolation.

The rake traverses made during this study are listed in Table 2. Most traverses with a coverage of 16 jet diameters in Z_v were made in two segments of 8 diameters each, with a major shift of the rake between segments so as to minimize data redundancy. A few traverses with 16-diameter coverage and all those with 12-diameter coverage were made with one-half jet diameter movements of the rake. After the eighth rake movement the lower probe repeated the location of the upper probe, but it was considered better to accept this redundancy than to complicate the computer program by providing an option for measuring either one or two probes depending upon the location of the probe during a traverse. Short traverses of irregular length were made when the probes were located under the wing; the traverse was terminated so as to avoid damage. Except for these irregular traverses, all of the traverses were set up so as to have an equal number of data points on either side of the vortex curve.

Wind tunnel scheduling demands made it impossible to make as complete a set of surveys for the intermediate lift case as for the other two. It was decided to get symmetry plane data only, and 12 traverses were made at $\lambda = .4$ and $\lambda = 8$ in addition to the 6 traverses at $\lambda = 6$ noted in Table 2. Regretably, the intermediate lift data for $\lambda = 4$ and $\lambda = 8$ were inadvertently lost from the data file while the central computer was being used for other purposes and the loss was not discovered until the model had been removed from the wind tunnel.

Approximately 6,000 data points were taken during the study. Each data point was generated by measuring 5 pressures on one of the probes for a total of over 30,000 pressures.

A log was kept on the time it took to run each survey. A traverse of 34 data points typically took 12 minutes to complete.

Rake Data Acquisition

The large amount of data to be taken and analyzed necessitated the use of an automated data acquisition system. Accordingly, a series of computer programs were written to control rake movement and the collection of rake data (pressures in the form of voltages). These programs were stored on disc in a central computer and down-loaded to a mini-computer (8k memory) at the wind tunnel as required. At suitable intervals, the voltage data were transferred to disc storage in the central computer. Because of core storage limitations in the mini-computer, input and output through the teletype terminal was not possible while the data were being taken. A limited diagnostic capability was

achieved through use of the crossbar scanner control; when the scanner was otherwise unemployed the setting of a specific channel number was used to indicate an error condition. A schematic of the data acquisition procedure is shown in figure 12, and some comments on the procedure are given below.

1) TUNLPR - This preliminary program was run at the beginning of a sequence of traverses, normally the beginning of a day. The readings, which established the full scale and zero of two signal conditioners and the zero offset of two transducers, were used later for calculation of pressures from the voltage output of the two data channels. Similar readings for a separate channel used to monitor plenum pressure were recorded manually at this time.

2) TUNLN - The measured value of $p_{o\infty}$ and p_{∞} output by this program allowed the operator to calculate the required value of jet plenum pressure precisely. He then made any necessary small correction to the approximate value of p_{o_p} set earlier. The paper tape input to JOBDTA was prepared prior to the runs by using an auxiliary program on the central computer which set up the required Y_v - Z_v planes (i.e. angles ϵ) using the results from the preliminary traverses. The rake was always moved one-half jet diameter along Z_v so that $\Delta X = (d_j/2) \sin \epsilon$ and $\Delta Z = (d_j/2) \cos \epsilon$. The number of steps was specified in the auxiliary program in conjunction with X_o and Z_o so that the traverse would be centered approximately on the vortex curve. The check entry gave the computer one of two options at the upper end of a traverse after the last data point had been taken: return the rake vertically downward to the lower limit switch for a check on the zero offset of Z, or else go to the next run number. After all of the entries had been made in JOBDTA, a test program TUNLH was down-loaded which provided verification of the entries in JOBDTA by printing them out on the teletype.

3) TUNL7 - This program controlled the acquisition of the rake data by controlling rake movement and data collection. User control of the program was possible at two points by the use of a sense switch on the computer panel. Pause #1 allowed the operator to control the initiation of a new traverse. Pause #2 allowed the operator to check visually on the location of the rake between steps if it were in a danger area near the wing. During the reading of the probe pressures the transducers were kept at the most sensitive scale factor possible by first reading each pressure once at a scale factor X 1.0 and then selecting the proper scale factor (X 1.0 or X 0.1 or X 0.01) for the data readings to follow. The averaging of 25 readings (each integrated over 1/60 second by the digital voltmeter) helped to minimize errors due to pressure fluctuations.

At the end of the day, a final program TUNL was used to check the contents of the disc data file by printing out the length of each record in the file. This gave a summary of the day's runs and allowed identification of any problems encountered (such as an interrupted run) so as to have a record of these during later data file searches. A typical print-out for two traverses containing 8 and 10 data points would be as follows:

Record #1	30 words (from TUNLPR)
Record #2	31 words (job from JOBDTA)
Record #3	8 words (p_{o_∞} and p_∞)
Record #4	80 words (4 data points)
Record #5	80 words (4 data points)
Record #6	31 words (next job)
Record #7	8 words (p_{o_∞} and p_∞)
Record #8	80 words (4 data points)
Record #9	80 words (4 data points)
Record #10	80 words (2 data points plus buffer)

If there were an odd number of steps in the traverse, the last 40 words in the final 80-word record corresponded to values left in the storage buffer of the computer from a previous reading. These were ignored in the data reduction.

Rake Data Reduction

The data reduction program first extracted the 32-word record of TUNLPR from the data file and also the part of the 31-word record written from JOBDTA which gave the necessary heading information such as run number, α, λ, and ϵ. The program next read the 8-word record containing output and identification voltages for tunnel stagnation and static pressure, reduced these to pressure using the TUNLPR data, and calculated V_∞ using density obtained from the tunnel pressure and temperature recorded in the remainder of the JOBDTA record. The 80-word records in the data file then were read and reduced to pressure using the TUNLPR data.

The 5 pressures for a particular probe next were input to the program PRNT, with the CALIB subroutine, which was furnished by NASA Langley Research Center. The output of this program was a value for U_v, V_v, and W_v (non-dimensionalized with the measured V_∞) plus a value of C_{p_o} and C_p for each probe location. The reduced data for each combination of α and λ for all traverses along the centerline and for all traverses in a Y_v - Z_v cross-section were output on a line printer and on 27 paper tapes. These paper tapes served as input for making vector plots of the velocity component data. In some of

the last traverses at maximum lift, $\lambda = 8$, problems were experienced when some of the vinyl tubes on one probe became clogged. The erroneous data were clearly evident in the vector plots and were edited out, as were all of the spurious data in the 80-word records containing readings from the storage buffer. Edited paper tapes were supplied to NASA Langley Research Center. Each paper tape contains the run number, α, λ, V_∞, ϵ, Y/d_j, X_o/d_j, Z_o/d_j, and the values of the 5 variables U_v/V_∞, V_v/V_∞, W_v/V_∞, C_{p_o}, and C_p at varying jet radii from the initial X_o, Z_o of the traverse.

The paper tapes of the centerline traverses were used in a plotting program utilizing a line printer in order to plot values of W_v versus Z_v and C_{p_o} versus Z_v. The resulting plots were faired by hand to determine the location of the maximum values of each variable which were used to determine the vortex curve and the jet centerline for each test condition.

The strength, Γ, and the half-spacing of the vortices, h, were calculated from the velocity measurements using the vortex filament model of Fearn and Weston (ref. 10). In this two-dimensional model, the contrarotating vortices are considered as two straight infinitely long vortex filaments placed a distance $2h$ apart. The measured upwash velocities (W_v) from the traverses in the symmetry plane ($Y = 0$) were used to calculate the parameters Γ and h for the filaments. It is assumed in the model that the component of freestream velocity in the $Y_v - Z_v$ plane is superimposed with that induced by the filaments to give the velocity component which is measured. The upwash velocity along the Z_v axis thus is written in terms of the unknowns Γ and h as

$$W_v = \frac{\Gamma h}{\pi(h^2 + Z_v^2)} - V_\infty \sin \epsilon$$

where ϵ is the known angle between the Z and Z_v axes and Z_v is the coordinate with respect to the vortex curve obtained earlier. The strength and the half-spacing were varied (ref. 15) to obtain a least square best fit of the above equation to the measured upwash velocities. The R.M.S. error for the fit, expressed as a percentage of the maximum upwash velocity measured in the traverse, was calculated to check the quality of the fit.

RESULTS AND DISCUSSION

The jet-off behavior of the wing-flap combination in lift, with varying angle of attack, is shown in figure 13. Also shown are the results from reference 13 for the wing alone and data for the NACA 0021 airfoil taken at a Reynolds number in excess of 3 million (ref. 16).

Curves of $\Delta L/T$ versus the more usual jet parameter $1/\lambda$ are shown in figure 14, where $\Delta L/T = (L_{jet\text{-}on} - L_{jet\text{-}off})/T$. The result for the minimum

lift case agrees well with the data of reference 13 for the wing alone at $\alpha = 0^\circ$ with the same jet located at 45% wing chord; it is considerably below the data of reference 13 with the jet located at 65% chord. Thus, for the minumum lift case, the lift interference of the jet at its location of 50% of the combined wing-flap chord was much like that of the same jet located at approximately the mid-chord of the wing alone. Note that, in the presentation of figure 14, zero interference lift corresponds to $\Delta L/T = 1.0$ and an interference lift loss corresponds to $\Delta L/T < 1.0$. For the minimum lift case, therefore, there was a small favorable lift interference at lower values of λ (as also was observed in ref. 13) while at the higher values of C_L there was always a lift loss due to the operation of the jet.

Figure 15 shows curves of $\Delta D/T$ and $\Delta PM/Td_j$ as a function of $1/\lambda$, where $\Delta D/T = (D_{jet\text{-}on} - D_{jet\text{-}off})/T$ and $\Delta PM/Td_j = (PM_{jet\text{-}on} - PM_{jet\text{-}off})/Td_j$. Zero interference drag corresponds to $\Delta D/T = 0$ and zero interference pitching moment is given by $\Delta PM/Td_j = 0$, where recall that pitching moment here is taken about the mid-chord of the wing. As has been discussed, the results presented are qualitative, but they do show that the interference drag due to the action of the jet was always positive (as also was noted in ref. 13). The interference drag data point for minimum lift with $1/\lambda = 0.25$ is questionable since the data of reference 13 for the wing alone show a sharp increase in interference drag with increasing values of $1/\lambda$ for the jet at $x/c = 0.45$. The interference drag for the wing alone at all angles of attack for the jet at $x/c = 0.45$ in reference 13 is somewhat greater than that measured in the present tests. The trend in interference pitching moment in figure 15 is the same as that for the wing alone. No wind tunnel wall corrections have been made for the force data presented.

Surface Pressures

The chordwise pressure distribution on the wing and flap in the plane of symmetry ($Y = 0$) with the jet off is shown in figure 16 for the minimum and maximum lift cases. The jet exit on the lower surface at 65% chord was situated in a constant adverse pressure gradient at minimum lift and in a region of essentially constant pressure at maximum lift. There is no evidence of wing or flap stall at maximum lift. During measurement of the wing surface pressures with the jet off, the jet exit was covered with a smooth fairing.

The two-dimensionality of the flow over the model with the jet off is illustrated by the spanwise pressure distribution on the wing lower surface at $x/c = 0.45$ shown in figure 17. The variation in spanwise pressure at minimum lift is almost identical to that measured for the wing alone at $\alpha = 0^\circ$ in reference 13, and is thought to be caused by surface irregularities. The non-uniformity in pressure near the sidewalls is attributed to the sidewall boundary layer and to the warpage of the flap at the ends.

Figure 18 shows typical interference surface pressure contours on the wing lower surface. No contours are presented for the wing upper surface since the effect of jet operation on the upper surface was quite small.

Interference pressure coefficients - $0.10 \leq \Delta C_p \leq 0$ were induced by the jet on the wing upper surface for minimum lift at $\lambda = 4$ and $\lambda = 8$. At maximum lift there was essentially zero interference at $\lambda = 4$ and a small positive interference $0 \leq \Delta C_p \leq 0.10$ on portions of the upper surface at $\lambda = 8$. Thus, as was true for the wing alone with $d_j/c = 0.10$ (ref. 13), the interference pressure distribution on the wing lower surface plays the dominant role. The pressure contours of figures 18(a) and 18(b) indicate that there is a large region of positive interference pressure upstream of the jet at $\lambda = 4$ which decreases in extent with increasing λ. The favorable interference lift measured at $1/\lambda = 0.25$ (fig. 14) is attributed to this positive interference pressure region at $\lambda = 4$. As λ increases, $\Delta L/T$ becomes more unfavorable because the positive region becomes progressively smaller. Around and to the rear of the jet exit are regions of negative interference pressure. The region of very large negative interference pressure in the wake of the jet is smaller near the jet at higher values of λ, while the lateral extent of the negative region is larger for higher values of λ with a resulting detrimental $\Delta L/T$ effect. At maximum lift (fig. 18(c) and 18(d)) the region of positive interference pressure is very small for all values of λ considered. The high negative interference pressure region in the wake is again smaller at higher values of λ, while the over-all negative interference pressure region enlarges with increasing λ. Thus, it may be concluded that the effect of lift on the wing surface pressures is to decrease the extent of the positive interference pressure region upstream of the jet, the relative decrease being greater for $\lambda = 4$ than for $\lambda = 8$. Also, increasing lift tends to pull the region of negative interference in the wake closer to the exit for a given λ. Lift has a weak effect on the extent of the negative interference pressure region to the side of the jet, this region being larger for larger values of λ.

Figure 19 gives the chordwise variation in interference pressure coefficient on the flap at $Y = 0$. For all lift cases, and for all values of λ, the interference on the upper surface of the flap was positive, i.e., the action of the jet was to increase the pressure and decrease the velocity on the flap upper surface downstream of the jet exit. The slot between the wing trailing edge and the flap apparently was less effective because of the blockage of the jet and also because the air passing through the slot was low-energy air from the wake region behind the jet. This behavior of the flap upper surface pressures with the jet on is opposite to that observed in the tests of reference 11. These tests, with a large jet located 0.64 chord-lengths below the wing, showed a lower pressure on the flap upper surface (30% chord NACA 4415 slotted Fowler flap deflected 40°) for all effective jet velocity ratios. This suggests that the interference effect of a jet on a flap may be sensitive to the vertical location of the jet exit relative to the flap.

Since the flap lies in the wake of the jet, it seems reasonable to expect that, for small flap deflections, the interference pressure on the lower surface of the flap directly behind the jet would be negative, as for a wing or a flat plate. However, such was not the case for $\delta = -5^\circ$ and $\delta = 0^\circ$, as can be seen in figure 19. The expected behavior was observed for $\delta = 15^\circ$,

with the ΔC_p changes on both the upper and lower surfaces suggesting an effective change in flap deflection angle. The chordwise pressure distributions measured on the flap gave no indication of flow separation for any jet operating condition.

The results of figure 19 also indicate that the interference pressure distribution on the flap at $Y = 0$ was quite insensitive to λ for a given C_L. Although the number of spanwise pressure taps on the flap was insufficient to allow any general conclusions to be drawn regarding spanwise interference, it was noted that at $Y/d_j = 1.37$ the interference effect on the upper surface at $\lambda = 8$ did not decrease appreciably at any C_L, while at $\lambda = 4$ the interference pressure coefficient at $Y/d_j = 1.37$ had decreased to about 30% - 50% of its magnitude on the centerline. The extent to which the flap effectiveness may be impaired because of the action of the jet cannot be evaluated from the limited data available, but the effect at large flap angles may be appreciable if the combination of higher pressures on the upper surface and lower pressures on the lower surface, as was observed here for $\delta = 15^\circ$, $Y = 0$, should persist over a significant portion of the flap span.

Velocity Field

A typical plot of the velocity vectors in a $Y_v - Z_v$ plane is shown in figure 20. The flow field induced by the jet vortex, as well as the vortex location, are readily apparent. Also shown in the figure is the center of the wing-flap wake as determined by examination of the total pressure distribution in the symmetry plane. Note that below the model wake (i.e. below the wing) the flow field is strongly influenced by the jet vortex. Above the wake the velocity vectors are essentially the component of the undisturbed freestream velocity in the $Y_v - Z_v$ plane. Thus, there was no significant influence of the jet vortex on the flow field above the wing-flap wake. The same behavior was observed at maximum lift at $\lambda = 4$. The traverses at $\lambda = 8$ did not cover the wake region.

Figure 21 presents typical velocity vector plots in $Y_v - Z_v$ planes. The coverage of these plots has been selected so as to emphasize the vortex region. The coordinate scales and the vector lengths (non-dimensionalized with V_∞) are the same for both of the plots. The magnitude of the velocity vectors shows how the vortex diffused for increasing values of X/d_j. The data at $Y/d_j = \pm 0.5$ and $Y/d_j = 0.0$ indicate that the flow field was essentially symmetrical about the plane $Y = 0$. The value of the vortex spacing and its variation with the various parameters may also be inferred from such plots. Figure 21 is primarily a pictorial representation of the flow field in and around the jet. The measured velocity fields may also be used to describe the behavior of the jet quantitatively; this is done in the subsequent sections.

Jet centerlines and vortex curves. Figure 22 shows the variation of the jet centerline (the locus of points of maximum C_{p_o} in the plane of symmetry $Y = 0$) as a function of C_L and λ. As might be expected from flat plate results, the jet penetrated further into the crossflow with increasing λ at minimum lift. The effect of lift was to increase the penetration of the jet for a given λ and, from the data for $\lambda = 6$, this increase was approximately linear with lift at a constant value of λ. As the lift was increased, the angle that the jet efflux made with the free-stream changed for 90° to 98° due to the change in wing angle of attack. However, equation (4) of reference 17 indicates that such a small change in injection angle has a small influence on the jet penetration and, at the values of X/d_j shown by the data points in figure 22, the penetration due to this effect would in fact be slightly reduced. Thus, the change in penetration observed with lift was not caused by the change in jet injection angle. Also shown in figure 22 is the empirical equation for the jet centerline as determined in reference 10 from experiments with a large flat plate. The maximum difference of one jet diameter between the empirical curves and the present results for minimum lift at all values of λ is not considered significant. What this implies is that there was no significant effect on the jet centerline when the infinite flat plate was replaced by a non-lifting finite chord wing, with resulting modifications in the flow field because of the change in boundary condition at $Z = 0$ (i.e., removal of the image vortex). It is the downwash in the flow field due to the lift which has a major effect on the jet centerline and which causes increased jet penetration with lift over that measured for the infinite flat plate case.

Figure 23 shows the behavior of the vortex curves (the projection of the vortex trajectories onto the symmetry plane $Y = 0$) as a function of C_L and λ. Again, as might be expected, at minimum lift the vortex curve moved to increasing values of Z/d_j as λ increased. The effect of lift was to displace the vortex curve downward for all values of λ and, from the results at $\lambda = 6$, the displacement is linear with C_L for a given λ. The effect of lift, then, was to displace both the jet centerline and the vortex curve downward. However, at $\lambda = 4$ the vertical spacing between the jet centerline and the vortex curve was almost independent of lift, whereas at $\lambda = 8$ the vortex curve was located further above the jet centerline with maximum lift than it was with minimum lift. Thus, the effect of lift on the vortex curve location was less pronounced as λ increased. Also shown in figure 23 is the vortex curve empirical equation given in reference 10 for the infinite flat plate. The effect on the vortex curve of replacing the flat plate with a body of finite chord at minimum lift is small. Again, as in the case of the jet centerline, the downwash due to lift has a major effect on the vortex curve and displaces it to larger values of Z/d_j than those observed from flat plate experiments.

Vortex spacing and strength. - Figure 24 shows the non-dimensional half-spacing, h/d_j, between the vortex centers as calculated from the vortex filament model of reference 10. The open data symbols indicate an RMS error of the fit to the measured upwash velocities of $\leq 8\%$ of the maximum W_v/V_∞

measured, and the cross-hatched data symbols indicate an RMS error between 8% and a maximum of 16%. The results of this calculation show that, at minimum lift, the half-spacing increased slightly as λ increased (as is also true for the flat plate case) and h increased with increasing X/d_j. The effect of lift was to increase h for all values of λ, with the larger increase occurring for the small values of X/d_j. The results at $\lambda = 6$ indicate that this increase may not be linear with C_L for a given λ. The results for the flat plate as read from the figures of reference 10 are also plotted in figure 24, and at minimum lift the spacing is slightly higher for the wing than for the flat plate.

Figures 24(a) and 24(c) also show the half-spacing of the vortex centers as inferred from vector plots like figure 21 and from similar plots presented in reference 10. Note that for the flat plate the half-spacing of the vortices predicted by the filament model tends to be higher (by approximately 20%) than the value for the vortex center half-spacing derived from the vector plots. A similar comparison of the present data shows that the filament model over-predicts the vortex half-spacing by about a factor of two. The filament model computer program used in the calculation of the results from the present tests was checked by using the available data in reference 10 for the distribution of W_v/V_∞; the calculated values of h/d_j (and of filament strength) agreed with those reported in reference 10. It is not known why the filament model predicts h more accurately for the flat plate case than for the wing case. Since both the vortex strength and the half-spacing are found as unknowns in the least square fit of the filament model, the values of vortex strength calculated from the present data may not be of the correct magnitude, but the trends in calculated vortex strength with the parameters of the experiment should still be valid.

Figure 25 shows the non-dimensional vortex strength, $\gamma = \Gamma/2d_jV_\infty$, calculated from the filament model as a function of C_L and λ. Again, the open data symbols indicate an RMS error of the fit of $\leq$ 8% of the maximum W_v/V_∞ measured, while the cross-hated data symbols indicate an RMS error between 8% and 16%. The results show that the vortex strength increased with increasing λ at minimum lift. The effect of lift was to increase the vortex strength with increasing C_L, larger increments being evident at lower values of λ. At $\lambda = 8$ the increment in strength persisted only up to $X/d_j = 16$. It is believed that the increase in vortex strength with lift is caused primarily by the increase in penetration of the jet with lift. However, this is not certain since at $\lambda = 6$ the penetration varied linearily with lift (fig. 22) while the vortex strength did not.

Also plotted in figure 25 are the vortex strength values read from the results presented in reference 10. The calculated strength at minimum lift using the same filament model is greater than the flat plate values at $\lambda = 4$ and less at $\lambda = 8$. This comparison with the flat plate may be invalid because of the discrepancy between the half-spacing results discussed earlier.

Also, the results for the minimum lift case should not necessarily be expected to agree with the flat plate case as did the penetration and vortex curve results. Recall the interference pressure distribution on the wing due to the jet flow. This interference implies changes in the spanwise loading on the wing even for the minimum lift case. These spanwise changes in circulation away from a constant (two-dimensional) value would imply the shedding of streamwise vorticity from the wing. This vorticity, in turn, may interact with the jet vortex so as to alter its strength even at minimum lift. A more thorough understanding of the effect of lift on the vortex strength can be achieved only after the application of the filament model to the wing case has been resolved.

CONCLUSIONS

An experimental investigation of a round turbulent jet issuing from a lifting two-dimensional wing in crossflow gives the following results:

1. There is a positive interference pressure region on the lower surface of the wing upstream of the jet exit. A small favorable lift interference measured at $\lambda = 4$ and $C_L = 0.034$ is attributed to the existence of this region. The effect of lift is to decrease the extent of this positive interference pressure region, with the relative decrease being greater for $\lambda = 4$ than for $\lambda = 8$. Lift has a weak effect on the negative interference pressure region to the side of the jet, this region being larger for larger values of λ.

2. For large flap deflection angles, the flap effectiveness may be impaired if the lifting jet is situated near the flap.

3. The wake of the wing divides the flow field into two regions at $\lambda = 4$. The flow field in the region below the wake (i.e. the region containing the jet) is strongly influenced by the jet vortices. The flow field above the wake is not significantly affected by these vortices.

4. At approximately zero lift, the penetration of the jet and the location of the vortices is about the same as that observed for a jet issuing from a large flat plate.

5. The jet centerline increases its penetration of the crossflow with increasing lift for all values of λ considered. At $\lambda = 6$ the variation with lift is linear.

6. With increasing lift, the vortex curve is displaced in the same direction as is the jet centerline. However, the displacement is less at $\lambda = 8$ than at $\lambda = 4$. At $\lambda = 6$ the variation of displacement with lift is linear.

7. The vortex filament model over-predicts the vortex half-spacing compared with that inferred from the velocity vector data. The results using the filament model indicate an increase in vortex half-spacing with increasing lift at all values of λ.

8. The vortex strength calculated from the filament model increases with increasing lift, with the increase being larger at lower values of λ. At $\lambda = 6$ the calculated increase is not linear with lift.

REFERENCES

1. Margason, R. J.; and Fearn, R. L.: Jet-Wake Characteristics and Their Induced Aerodynamic Effects on V/STOL Aircraft in Transitional Flight. NASA SP 218, 1969, pp. 1-18.

2. Margason, R. L.: Review of Propulsion - Induced Effects on Aerodynamics of Jet/STOL Aircraft. NASA TN D-5617, 1970.

3. Keffer, J. G.; and Baines, W. D.: The Round Turbulent Jet in a Cross Wind. Journal of Fluid Mechanics, Vol. 15 Pt. 4, 1963, pp. 481-496.

4. Bradbury, L. J. S.; and Wood, N. M.: The Static Pressure Distribution Around a Circular Jet Exhausting Normally from a Plane Wall into an Airstream. TN Aero 2978, British Royal Aircraft Establishment, 1964.

5. Mosher, D. K.: An Experimental Investigation of a Turbulent Jet in a Crossflow. Ph.D. Thesis, Georgia Institute of Technology, Atlanta, Georgia, 1970.

6. Wooler, P. T.: On the Flow Past a Circular Jet Exhausting at Right Angles from a Flat Plate or a Wing. Journal of the Royal Aeronautical Society, Vol. 71, pp. 216-218, 1967.

7. Kamotani, Y.; and Greber, I.: Experiments on a Turbulent Jet in a Cross Flow. AIAA Journal, Vol. 10, No. 11, pp. 1425-1492, 1972.

8. Antani, D. L.: An Experimental Investigation of the Vortices and the Wake Associated with a Jet in Crossflow. Ph.D. Thesis, Georgia Institute of Technology, Atlanta, Georgia, 1977.

9. Thompson, A. M.: The Flow Induced by Jets Exhausting Normally from a Plane Wall into an Airstream. Ph.D. Thesis, Univ. of London, 1971.

10. Fearn, R.; and Weston, R. P.: The Vorticity Associated with a Jet in Crossflow. AIAA Journal, Vol. 12, No. 12, pp. 1666-1671, 1974.

11. Carter, A.: Effects of Jet-Exhaust Locations on the Longitudinal Aerodynamic Characteristics of a Jet/STOL Model. NASA TN D-5333, 1969.

12. Wooler, P. T.; Burghart, G. H.; and Gallagher, J. T.: The Pressure Distribution on a Rectangular Wing with a Jet Exhausting Normally into an Airstream. AIAA Journal of Aircraft, Vol. 4, No. 6, pp. 537-543, 1967.

13. Mikolowsky, W.T.: An Experimental Investigation of a Jet Issuing from a Wing in Crossflow. Ph.D. Thesis, Georgia Institute of Technology, Atlanta, Georgia, 1972. (University Microfilms #72-26312). A condensed version of this work appears in AIAA Journal of Aircraft, Vol. 10, No. 9, pp. 546-553, 1973.

14. Sinclair, A. R.; and Robins, A.W.: A Method for the Determination of the Time Lag in Pressure Measuring Systems Incorporating Capillaries. NACA TN 2793, 1952.

15. Nielsen, K. L.: Methods in Numerical Analysis, 2nd ed., Macmillan, 1964, pp. 308-311.

16. Jacobs, E. N.: Tests of Six Symmetrical Airfoils in the Variable Density Wind Tunnel. NACA TN 385, 1931.

17. Margason, R. J.: The Path of a Jet Directed at Large Angles to a Subsonic Free Stream. NASA TN D-4919, 1968.

TABLE 1

FLAP PRESSURE TAP LOCATIONS

Spanwise		Chordwise	
Upper Surface	Lower Surface	Upper Surface	Lower Surface
Y/d_j	Y/d_j	x/c_f (%)	x/c_f (%)
0	0	5	0
1.37	0.69	10	7.5
	1.37	15	15
	2.07	31	31
		45	45
		55	55
		65	65

(For wing pressure tap locations see reference 13)

TABLE 2

SUMMARY OF RAKE TRAVERSES

C_L	λ	Y/d_j	X/d_j for each Y/d_j
0.034	4	0.0	4, 5, 6, 8, 10, 12, 14, 16, 20, 25, 30, 35
		-0.5, 0.0, 0.5 1.0, 1.5, 2.0, 2.5, 3.0, 3.5, 4.0, 4.5, 5.0, 5.5	4, 8, 14
	6	0.0	8, 14, 20, 25, 35
	8	Same a $\lambda = 4$	Same as $\lambda = 4$
1.24	6	0.0	4, 8, 14, 20, 25, 35
2.45	4	0.0	4, 5, 6, 8, 10, 12, 14, 16, 20, 25, 30, 35
		-0.5, 0.0, 0.5, 1.0, 1.5, 2.0, 2.5, 3.0, 3.5, 4.0, 4.5, 5.0, 5.5	4, 8, 14
	6	0.0	4, 8, 14, 20, 25, 35
	8	Same as $\lambda = 4$	Same as $\lambda = 4$

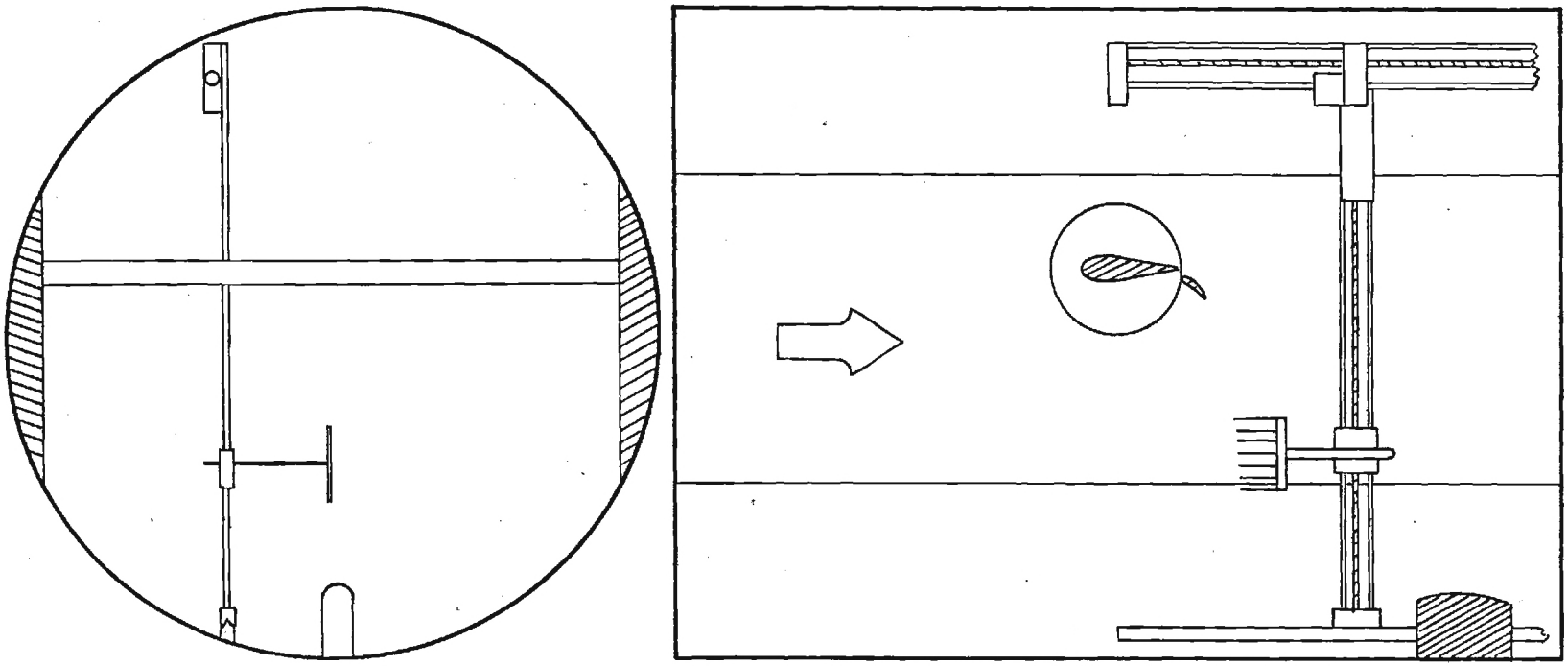

Figure 1. - Model and actuator in wind tunnel test section.

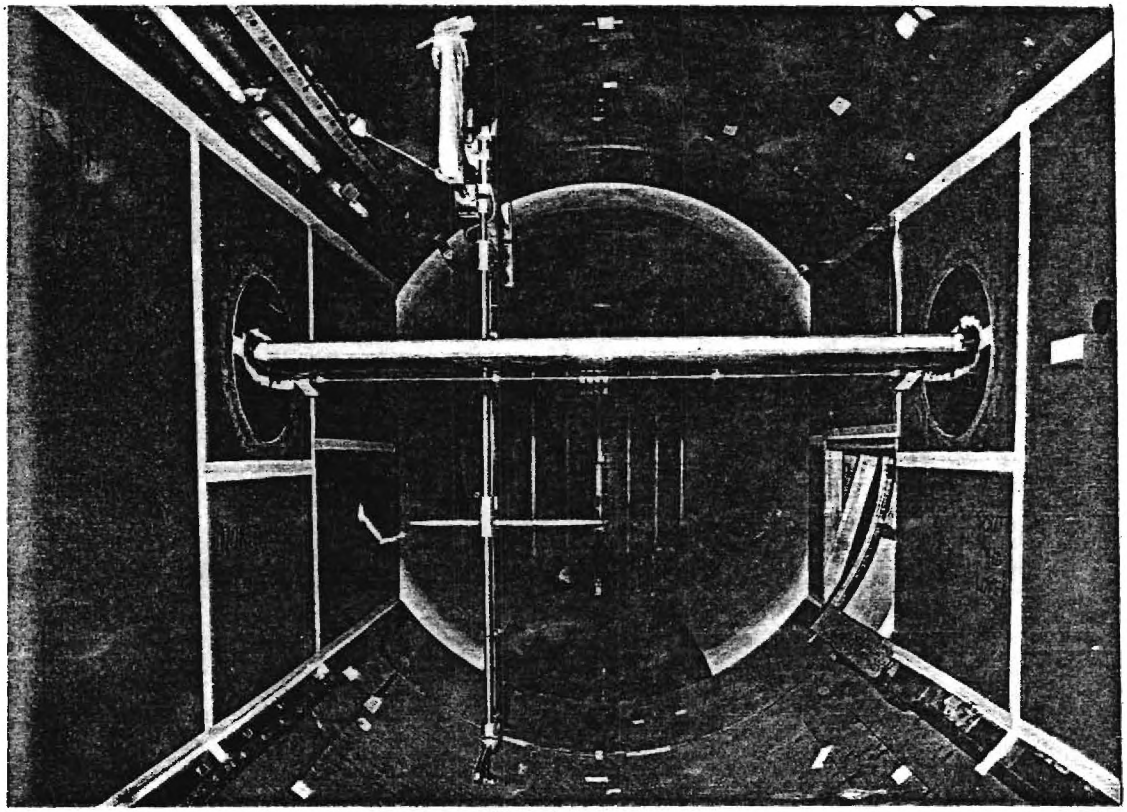

(a) View looking downstream

Figure 2. - Photograph of test section with model and actuator installed.

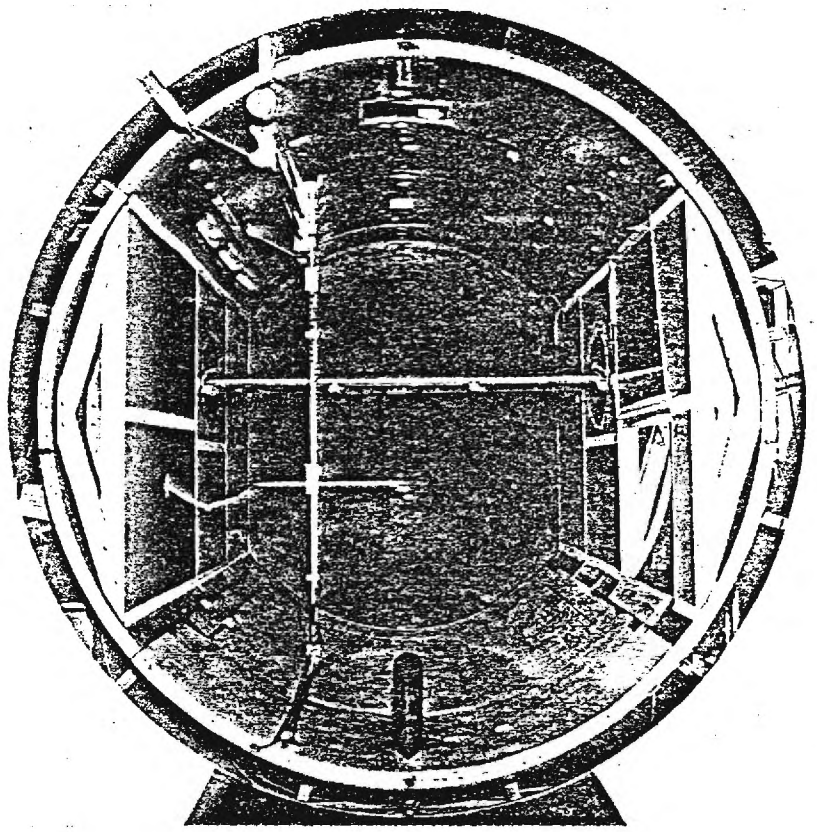

(b) View looking upstream.

Figure 2. - Concluded.

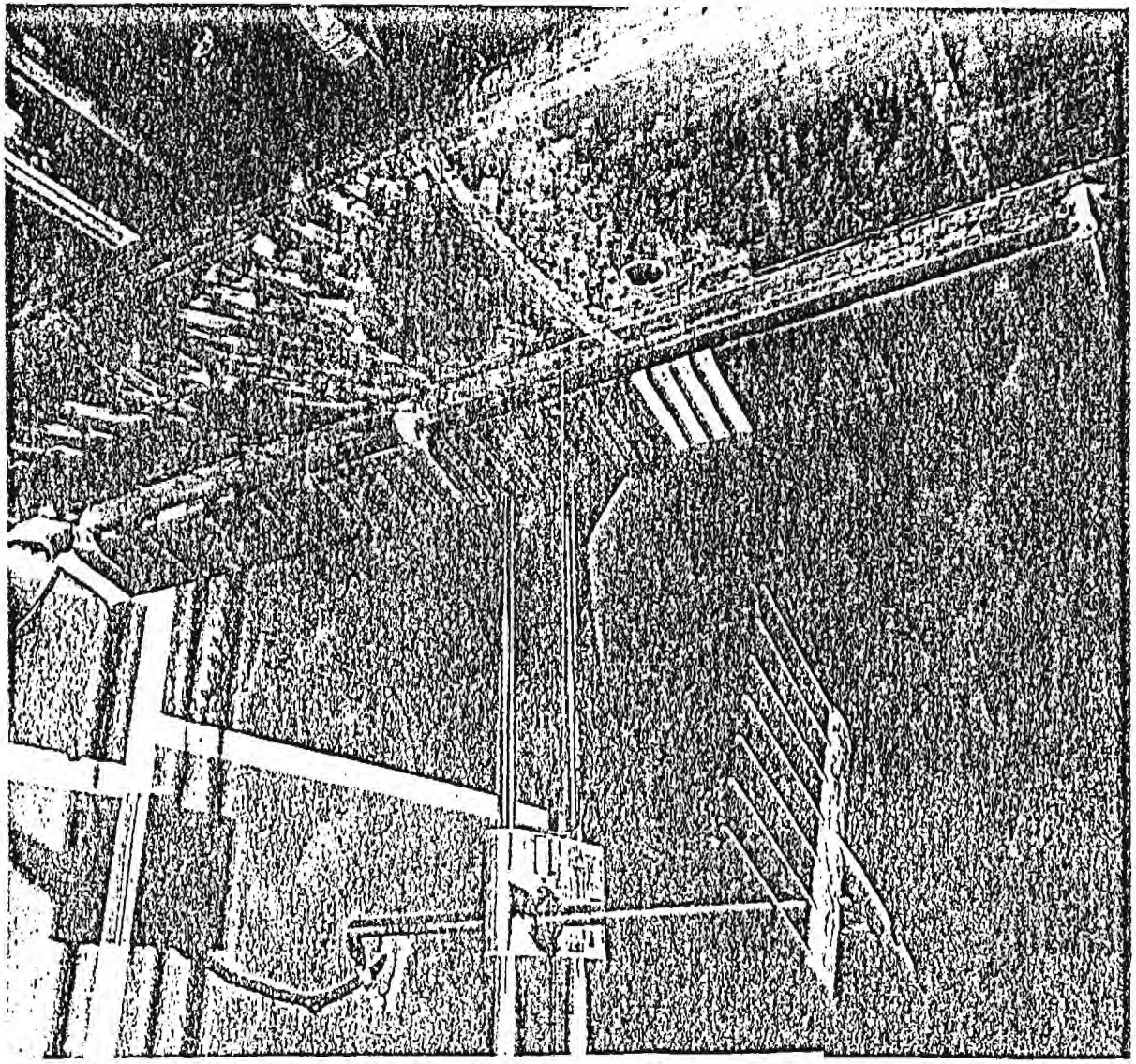

Figure 3. - Wing and flap.

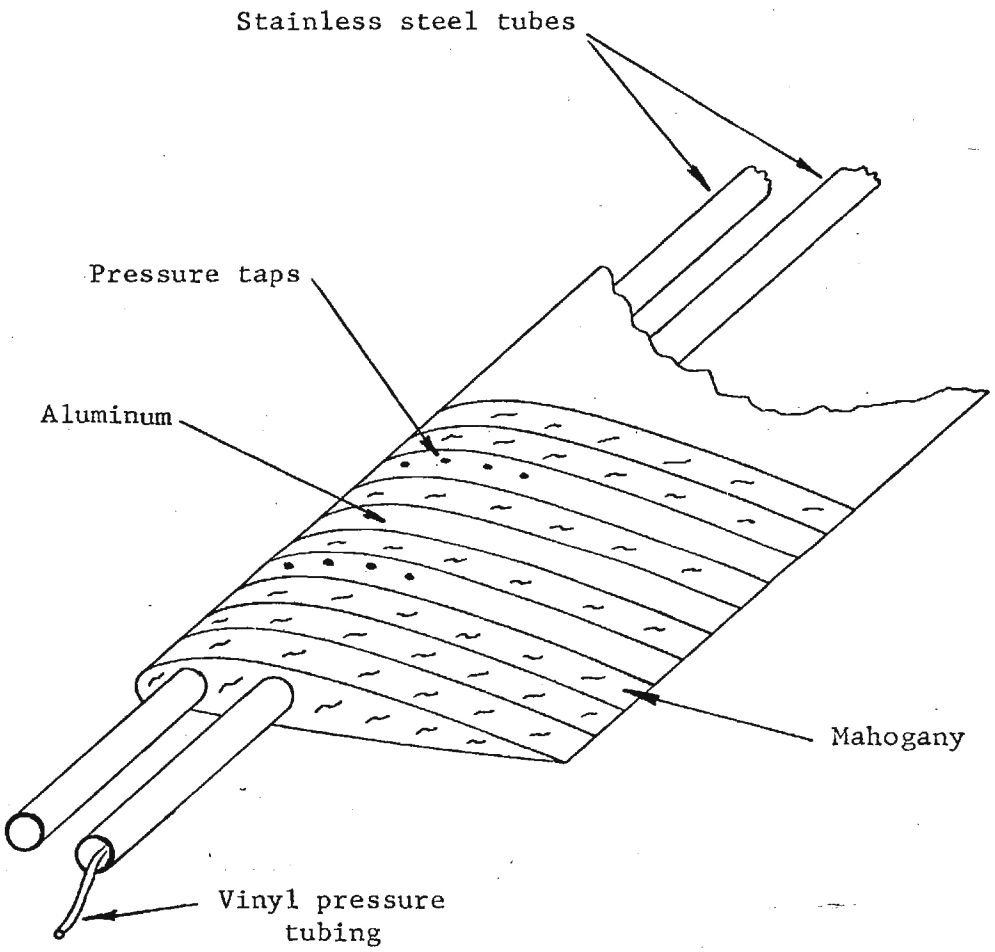

Figure 4. - Flap construction.

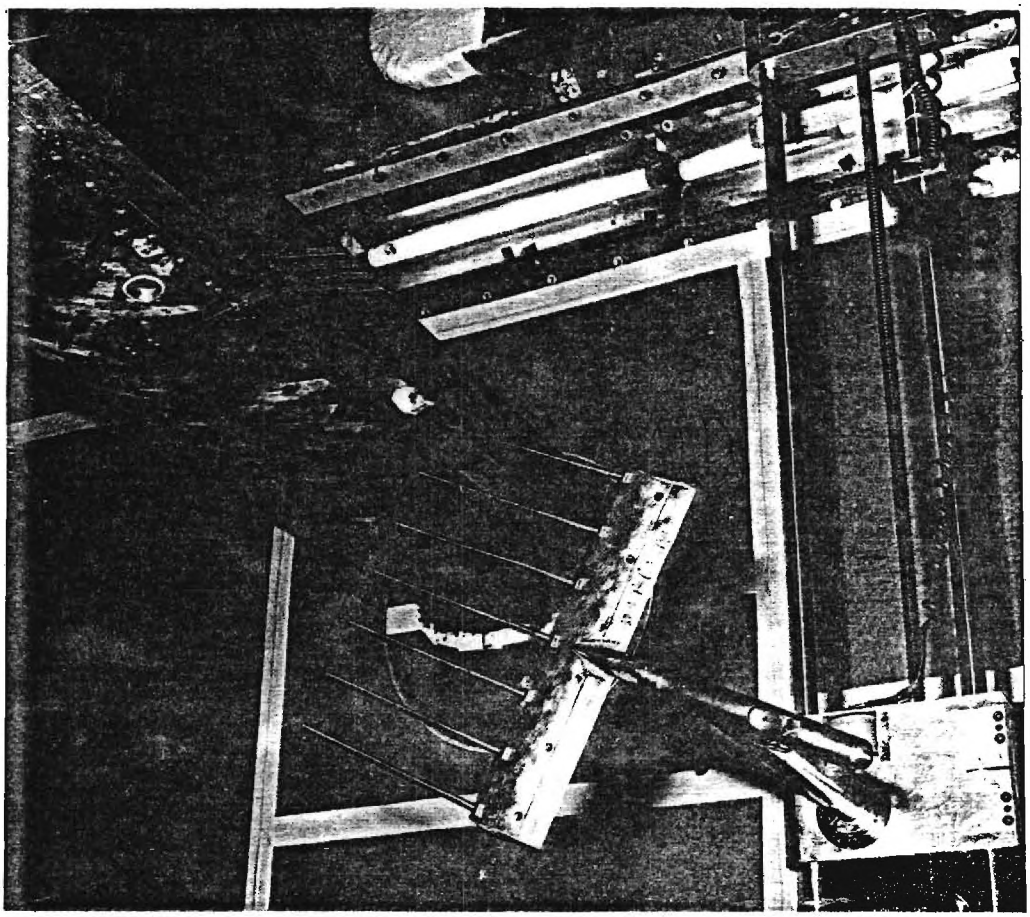

Figure 5. - Probe rake and rake-holder.

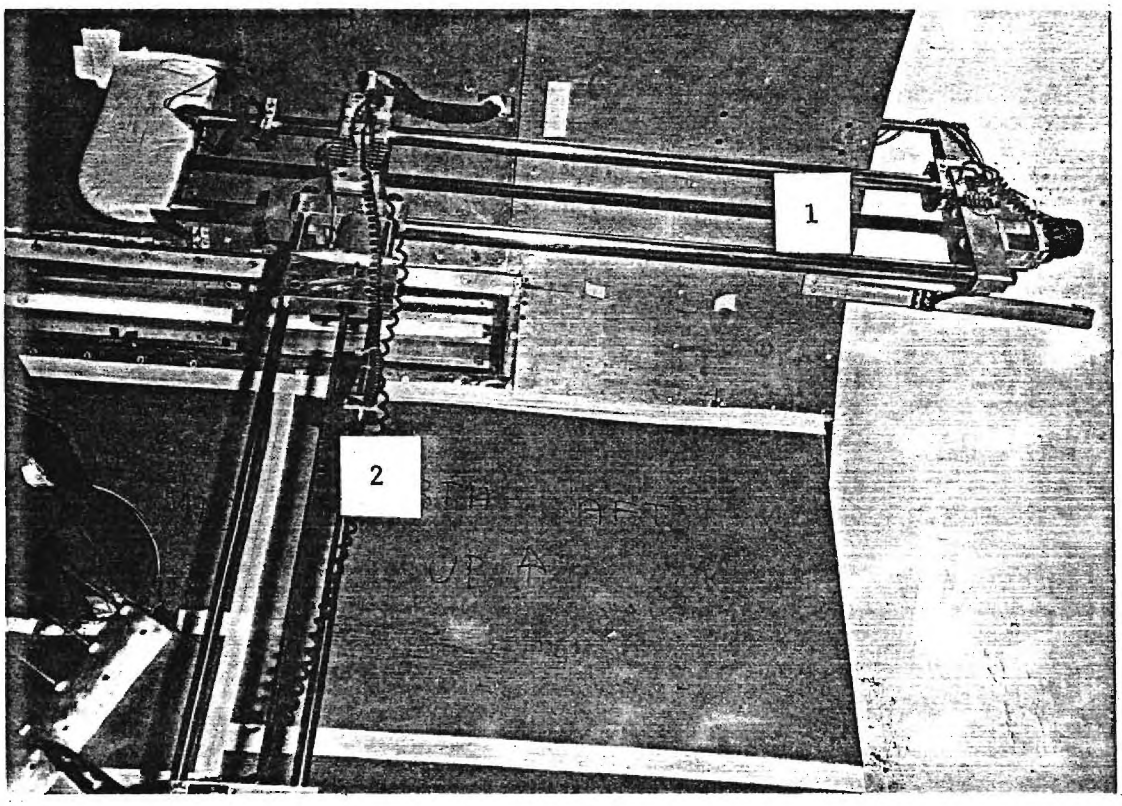

Figure 6. - Actuator installed in test section (view from below).

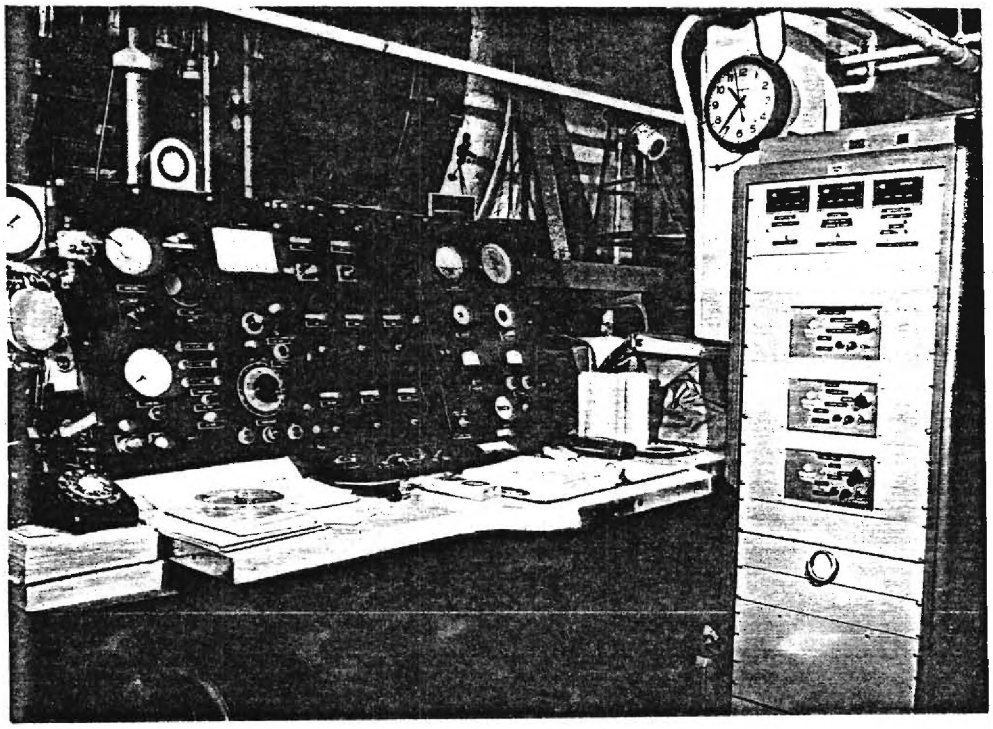

Figure 7. - Wind tunnel operating console and stepping motor controls.

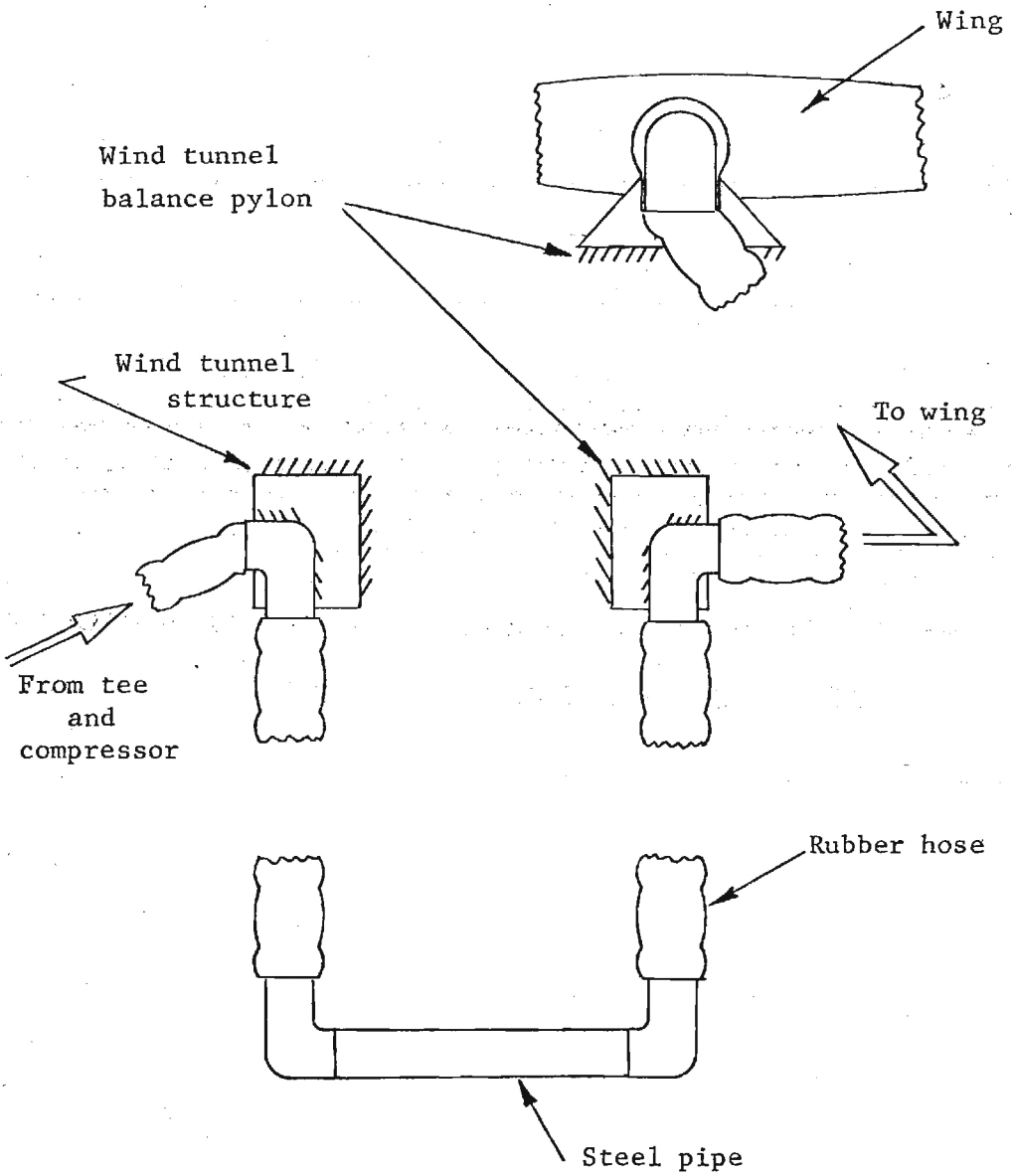

Figure 8. - Jet air supply line schematic.

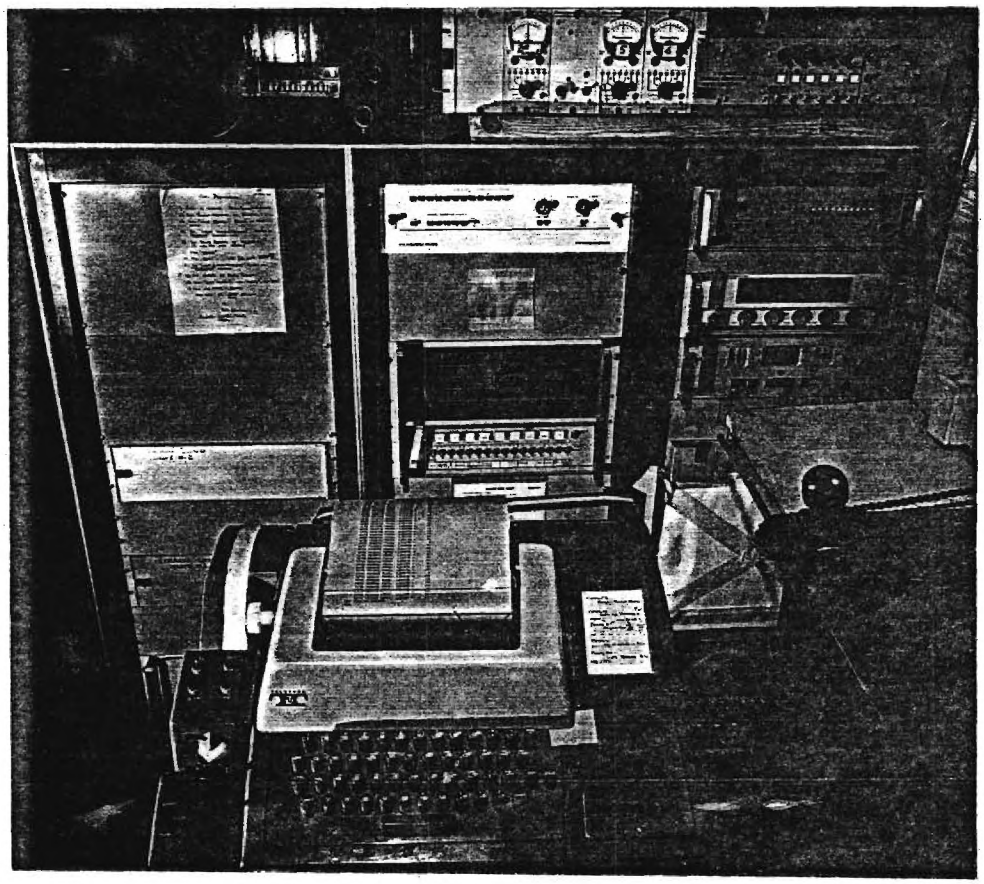

Figure 9. - Data acquisition system for rake pressures.

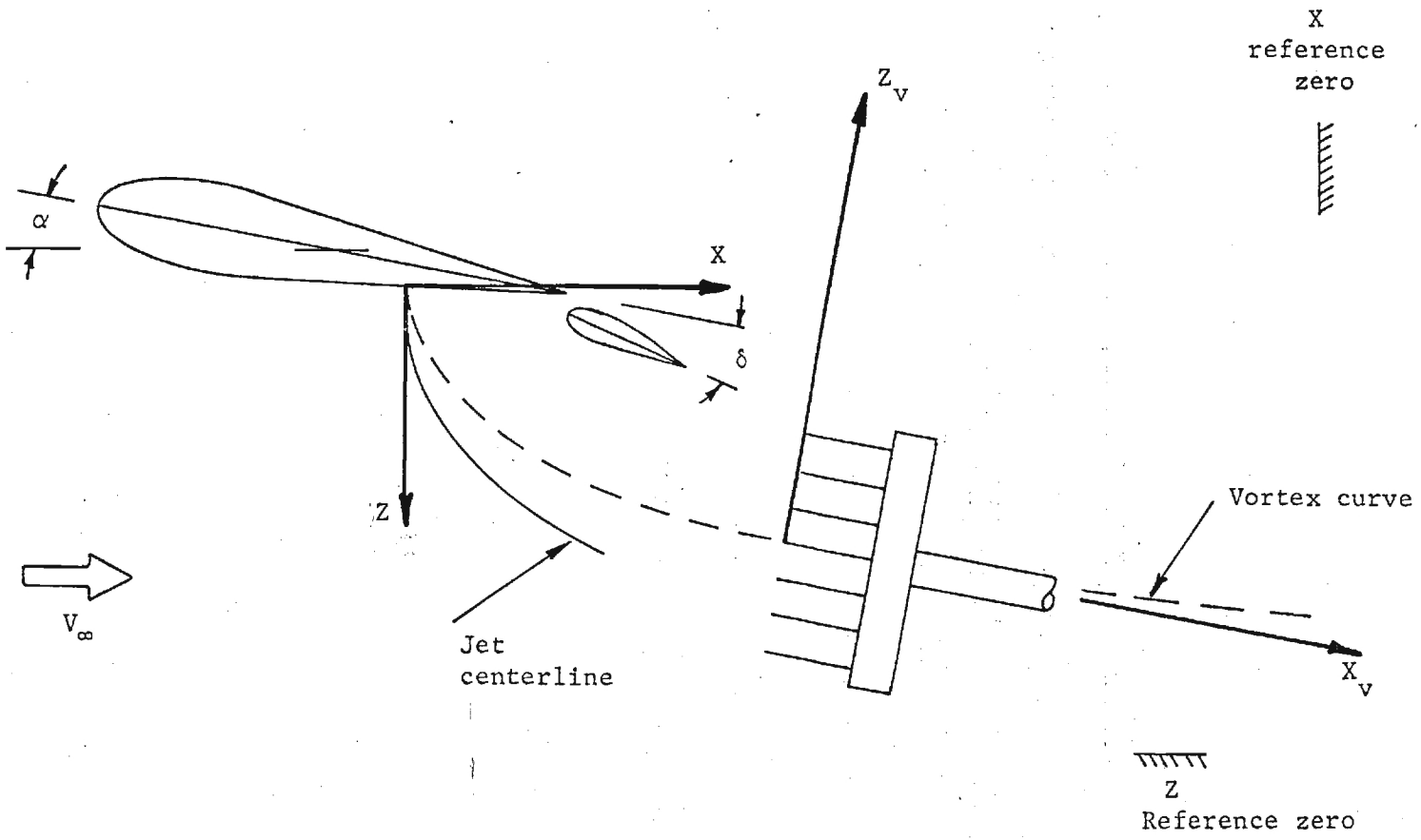

Figure 10. - Axis systems and nomenclature.

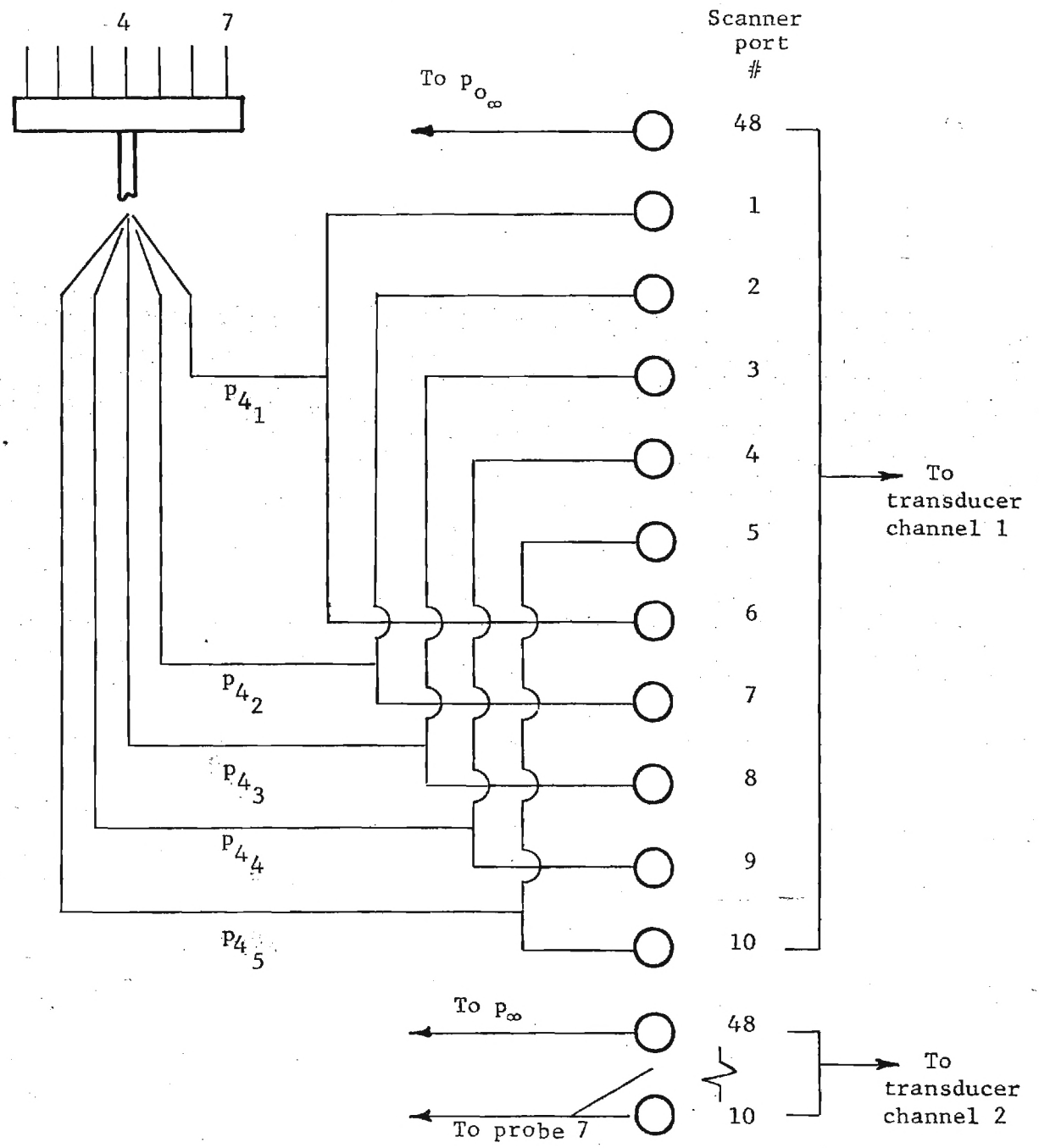

Figure 11.- Rake pressure tubing schematic.

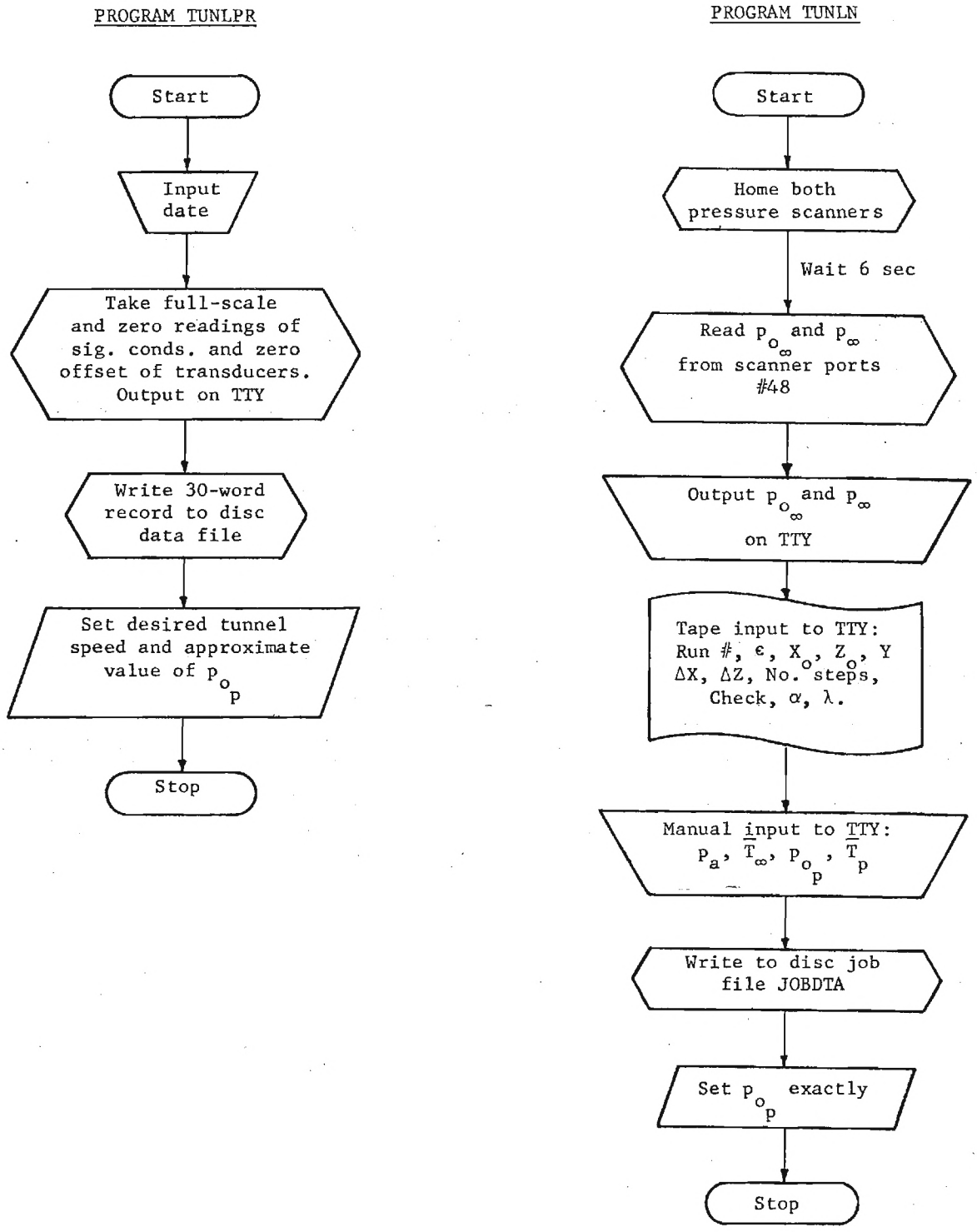

Figure 12. - Data Acquisition Flow Chart

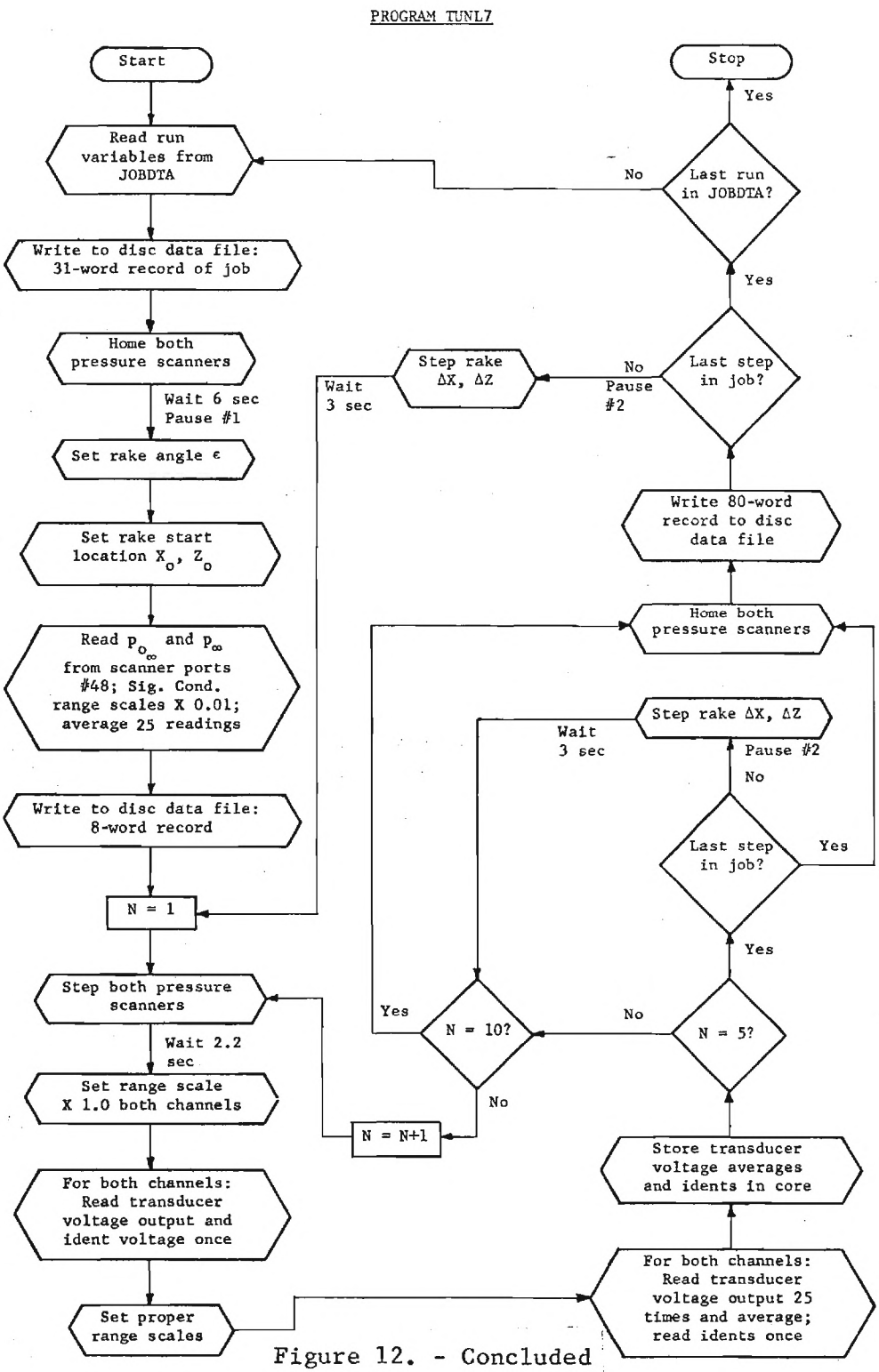

Figure 12. - Concluded

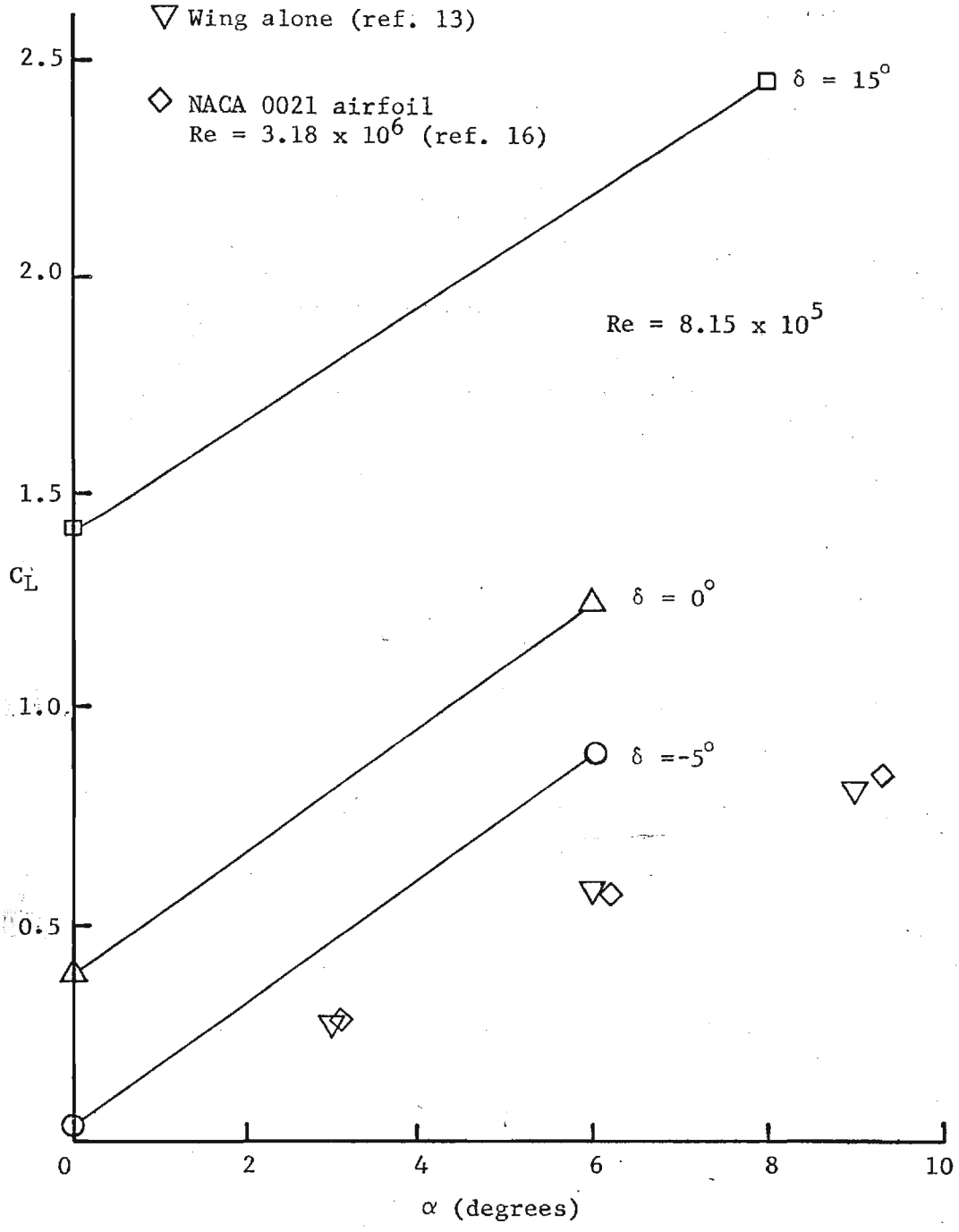

Figure 13. - Lift coefficient for wing-flap.

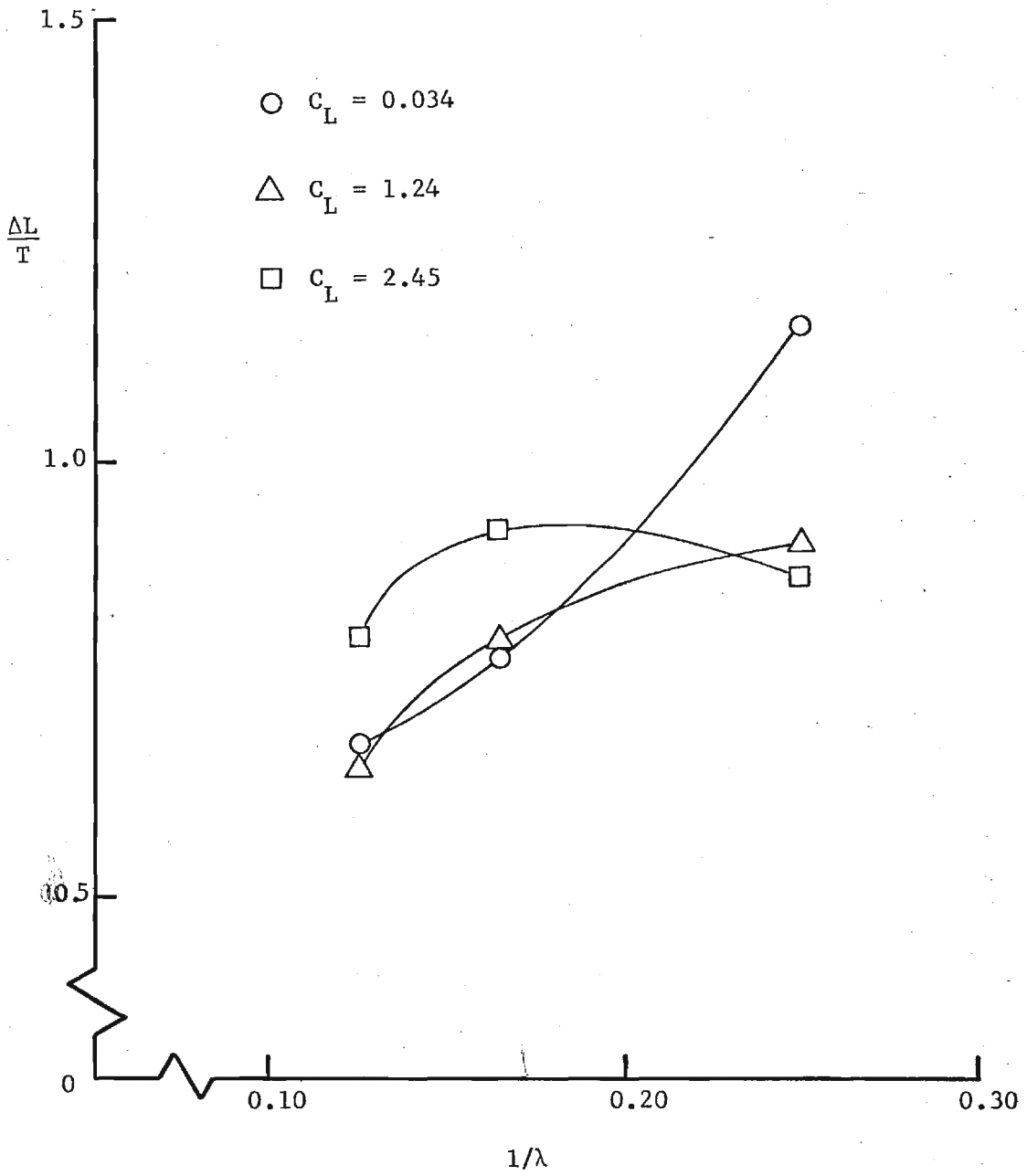

Figure 14. - Variation of interference lift with lift coefficient.

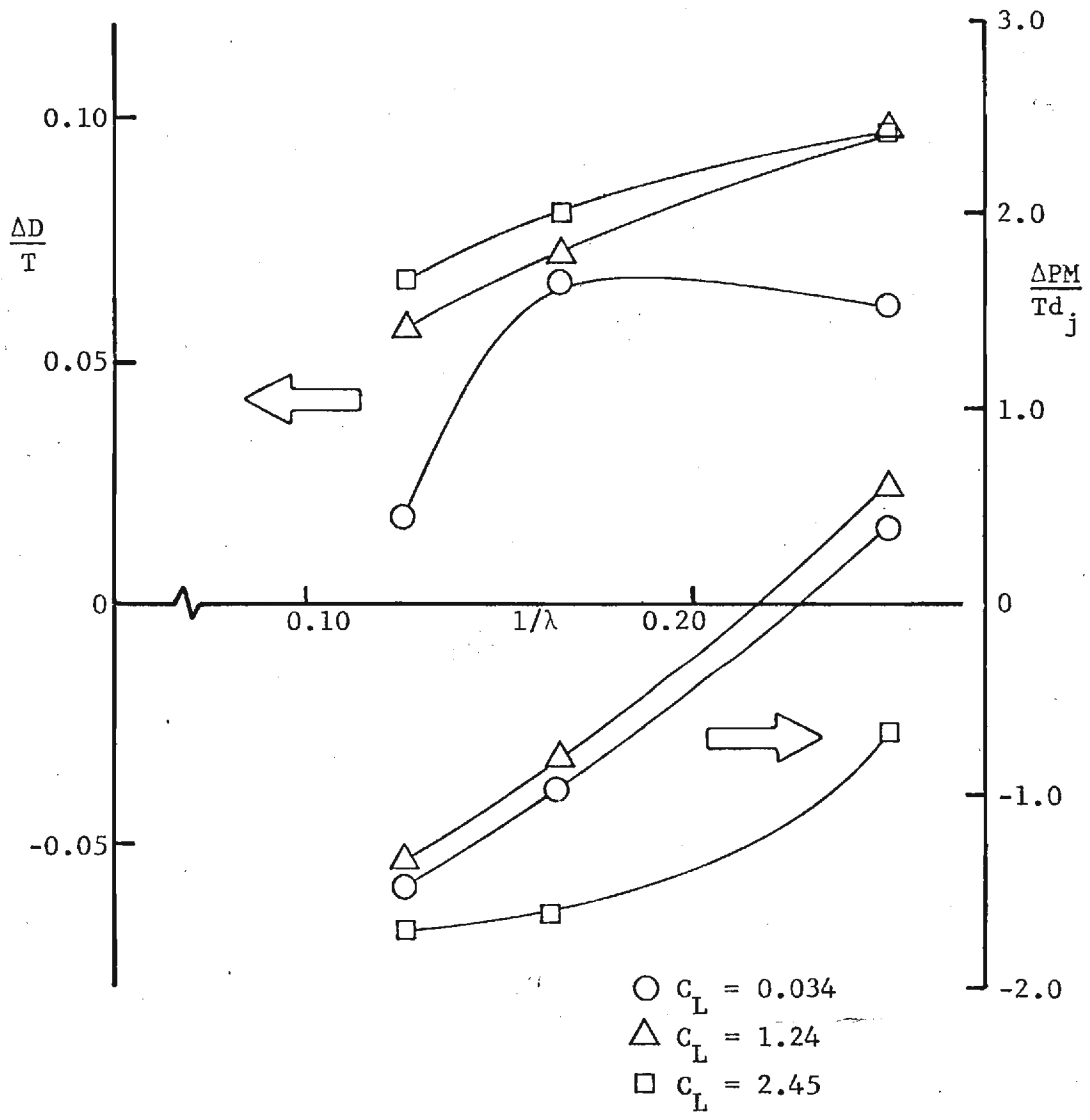

Figure 15. - Variation of interference drag and pitching moment with lift coefficient.

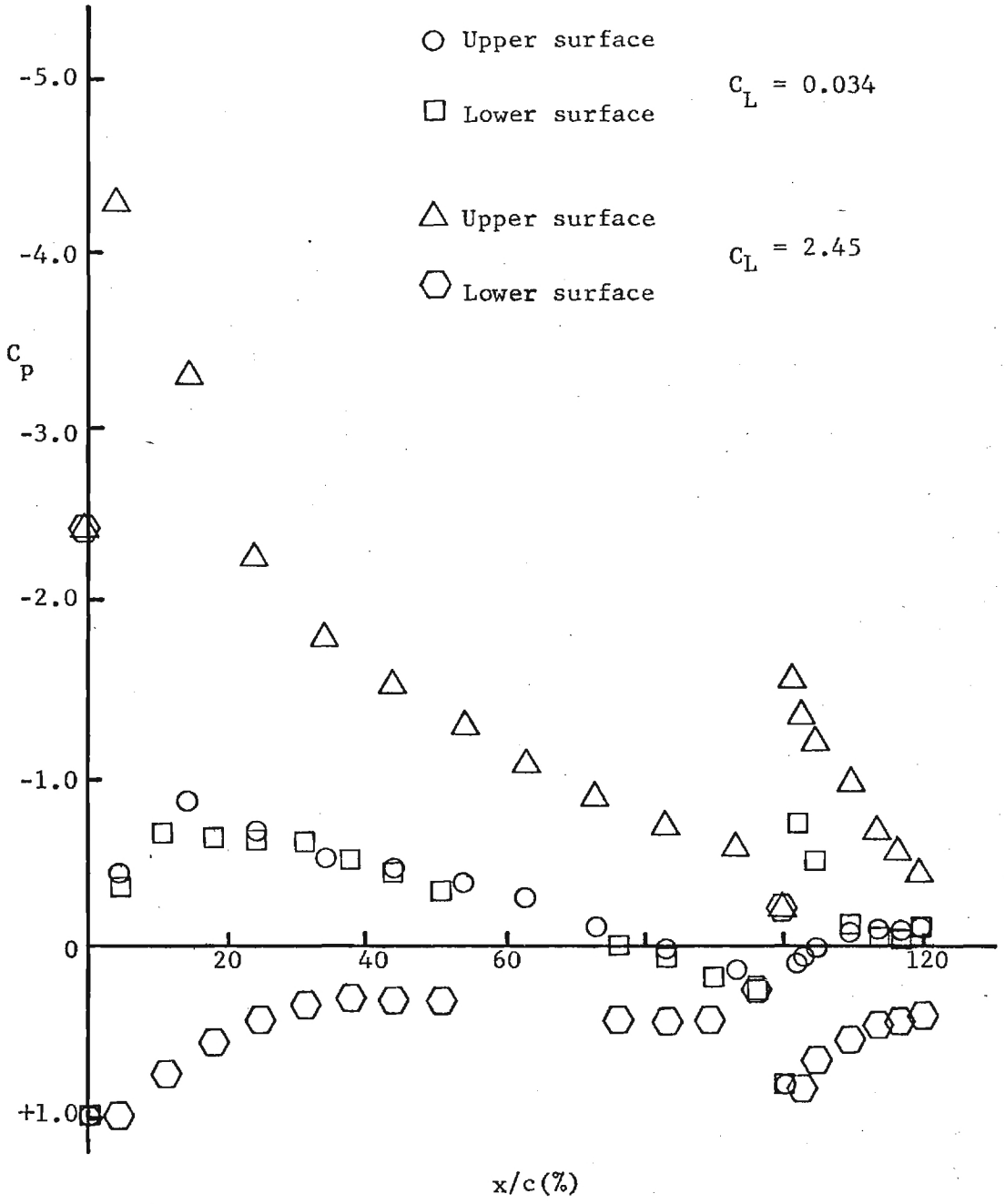

Figure 16. - Chordwise pressure distribution on wing and flap with jet off. Y = 0.

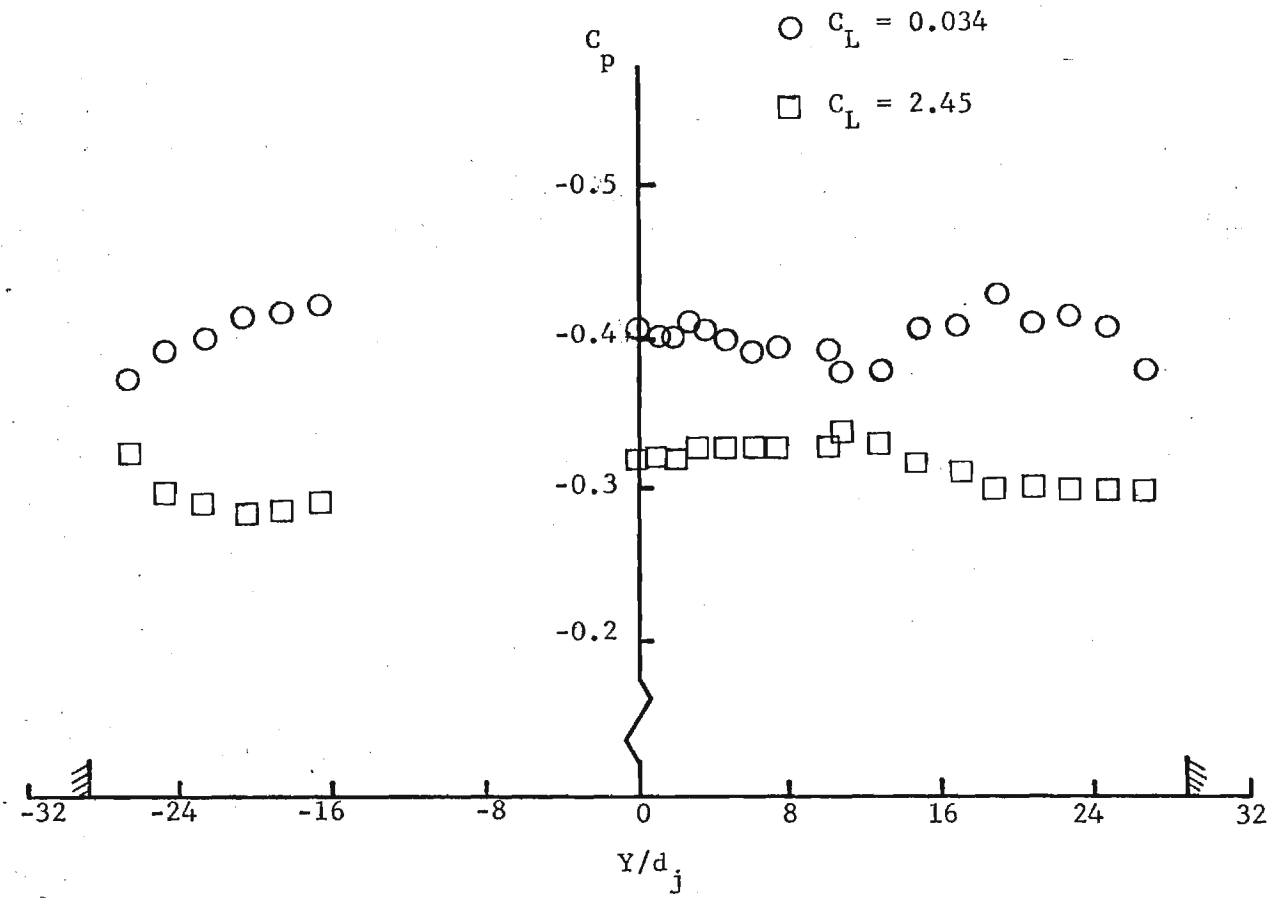

Figure 17. - Spanwise pressure distribution on wing lower surface at x/c = 0.45 with jet off.

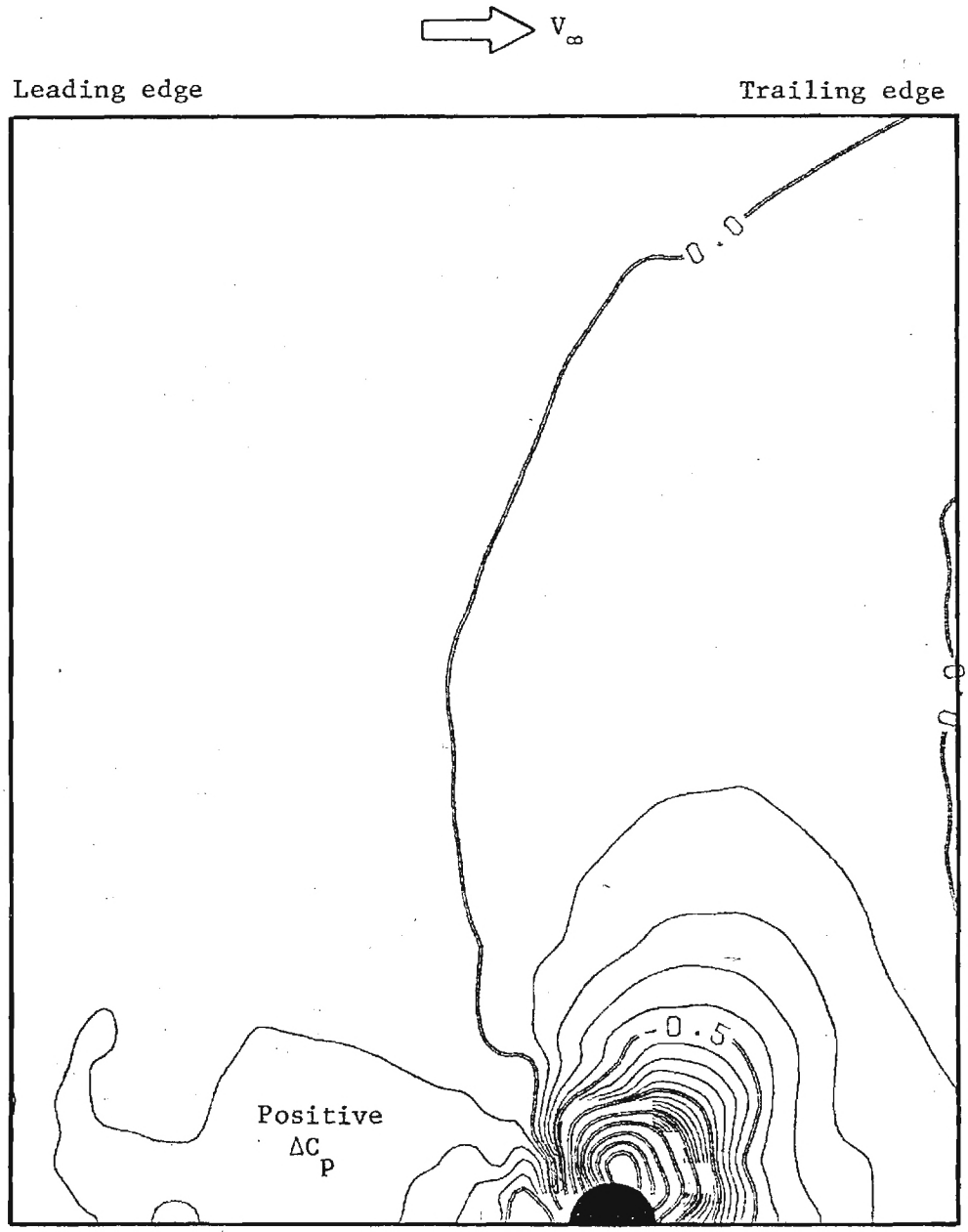

(a) $C_L = 0.034$, $\lambda = 4$

Figure 18. - Variation of wing interference pressure distribution with jet velocity ratio and lift coefficient.

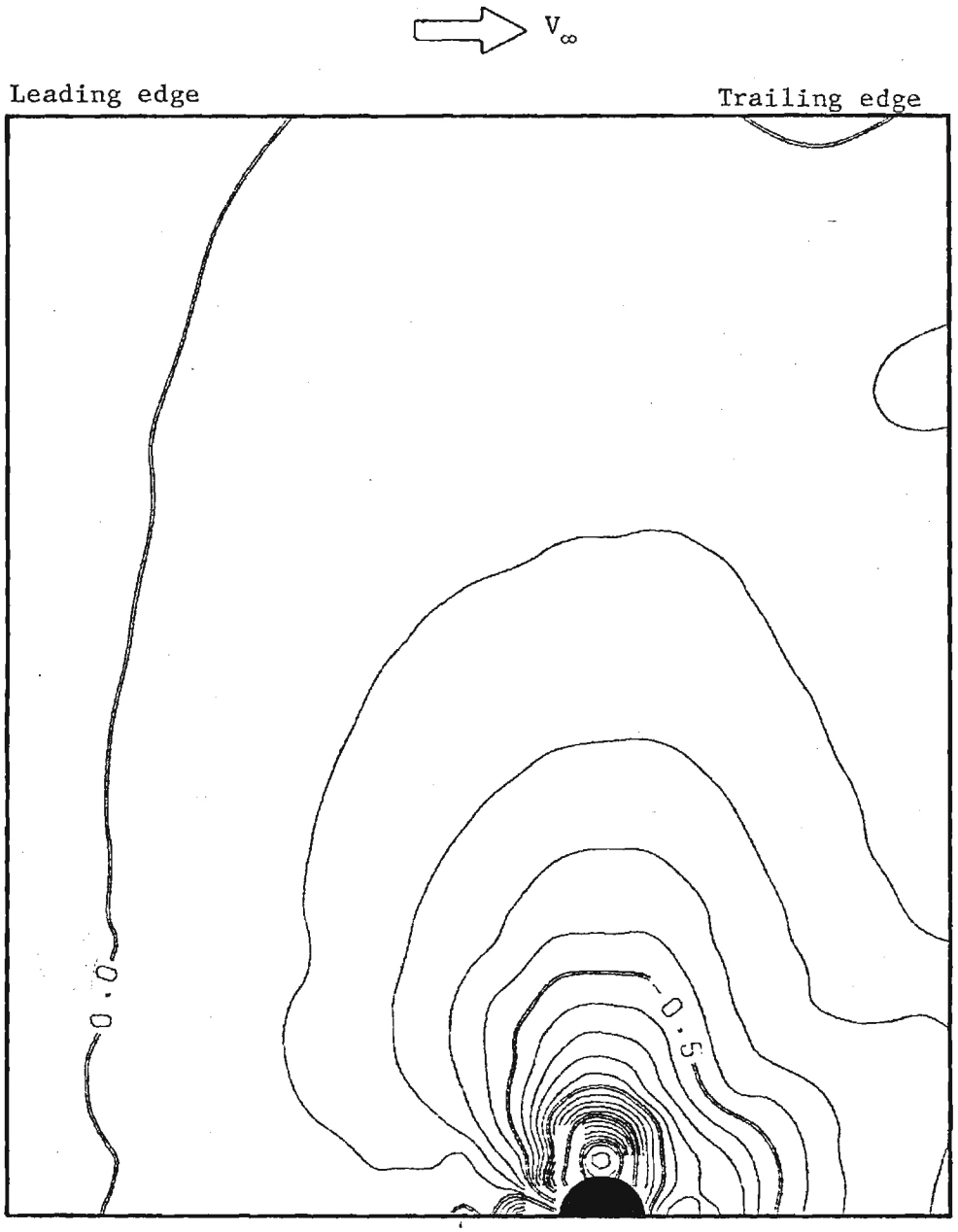

(b) $C_L = 0.034$, $\lambda = 8$

Figure 18. - Continued

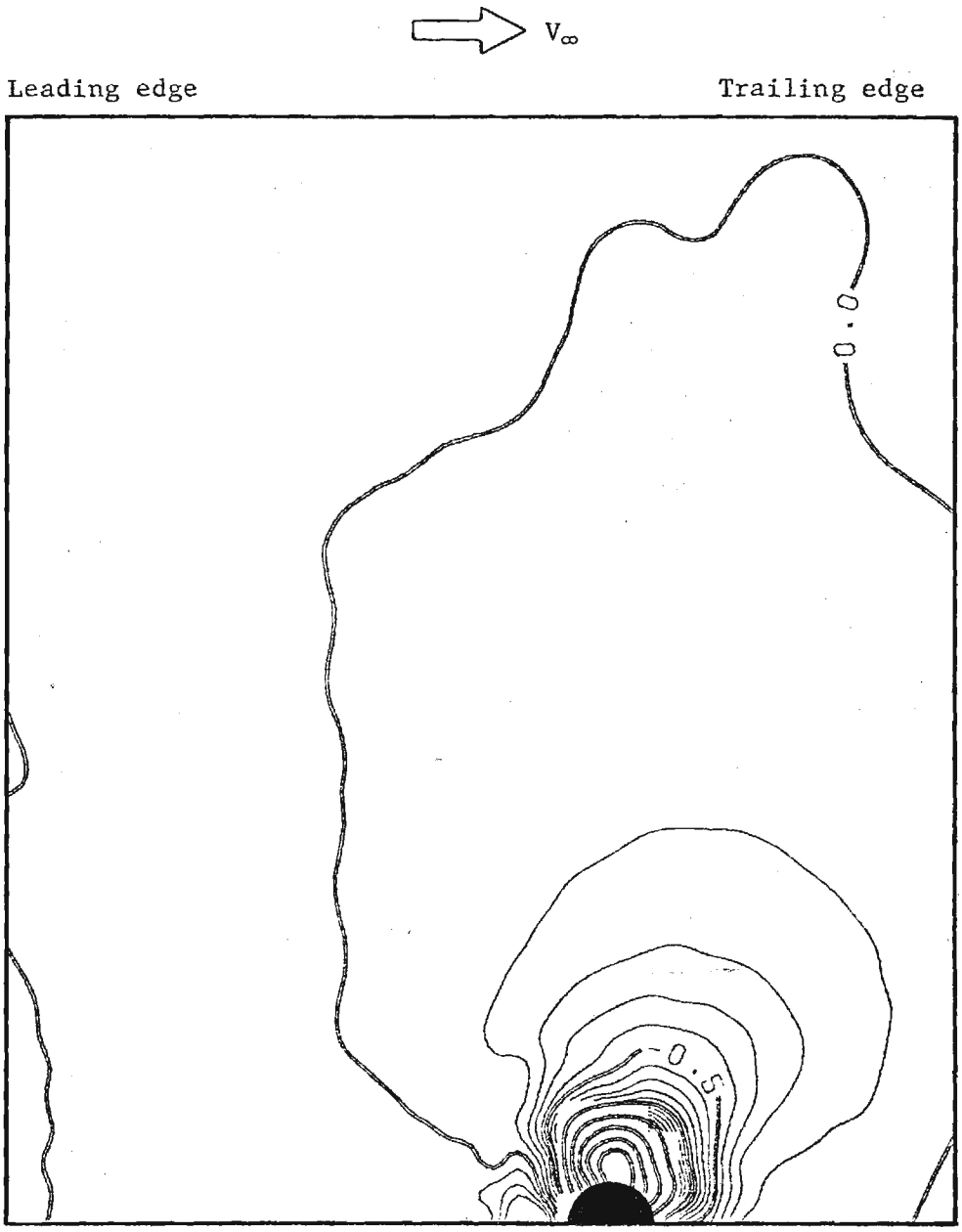

(c) $C_L = 2.45, \quad \lambda = 4$

Figure 18. - Continued

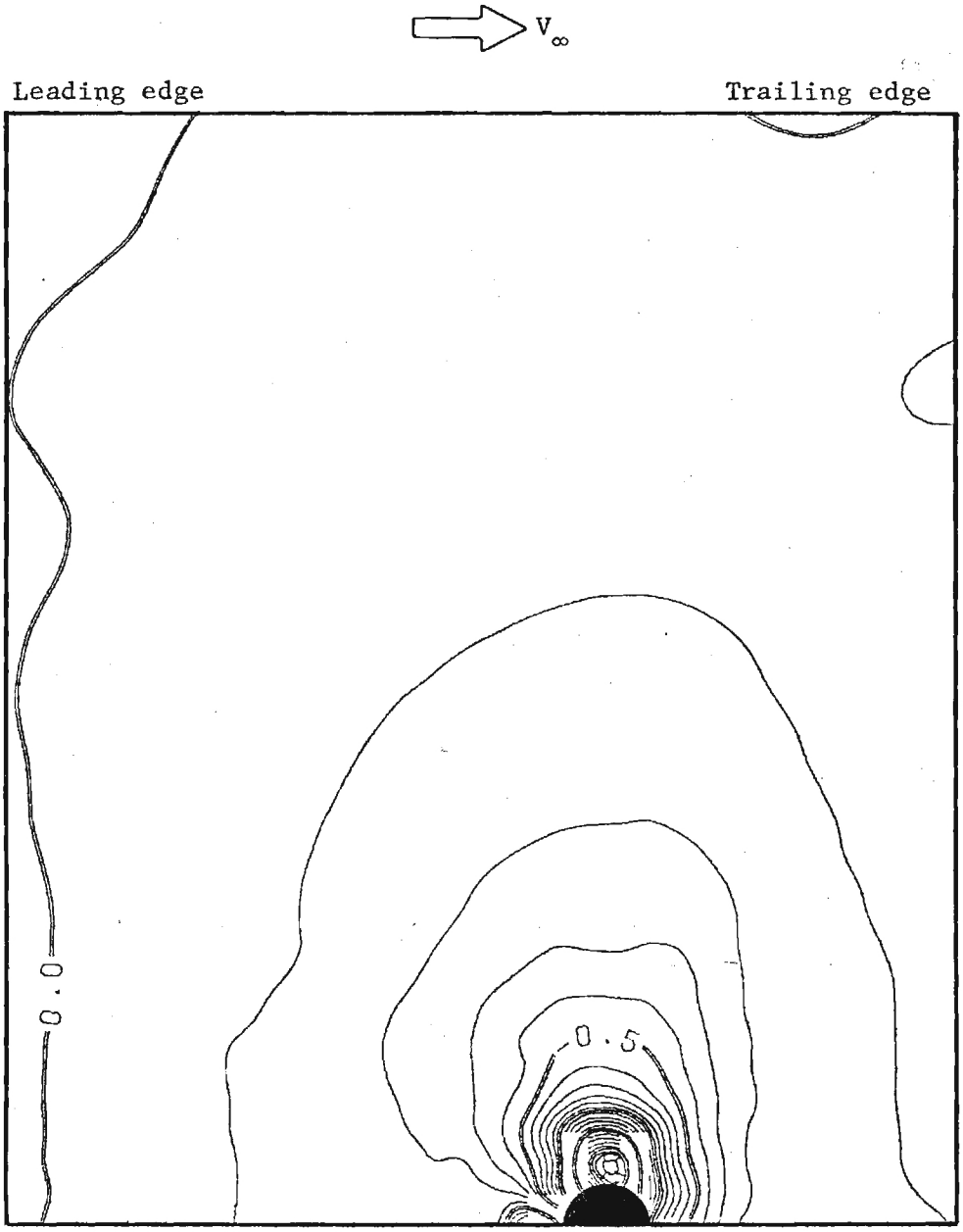

(d) $C_L = 2.45, \quad \lambda = 8$

Figure 18. - Concluded

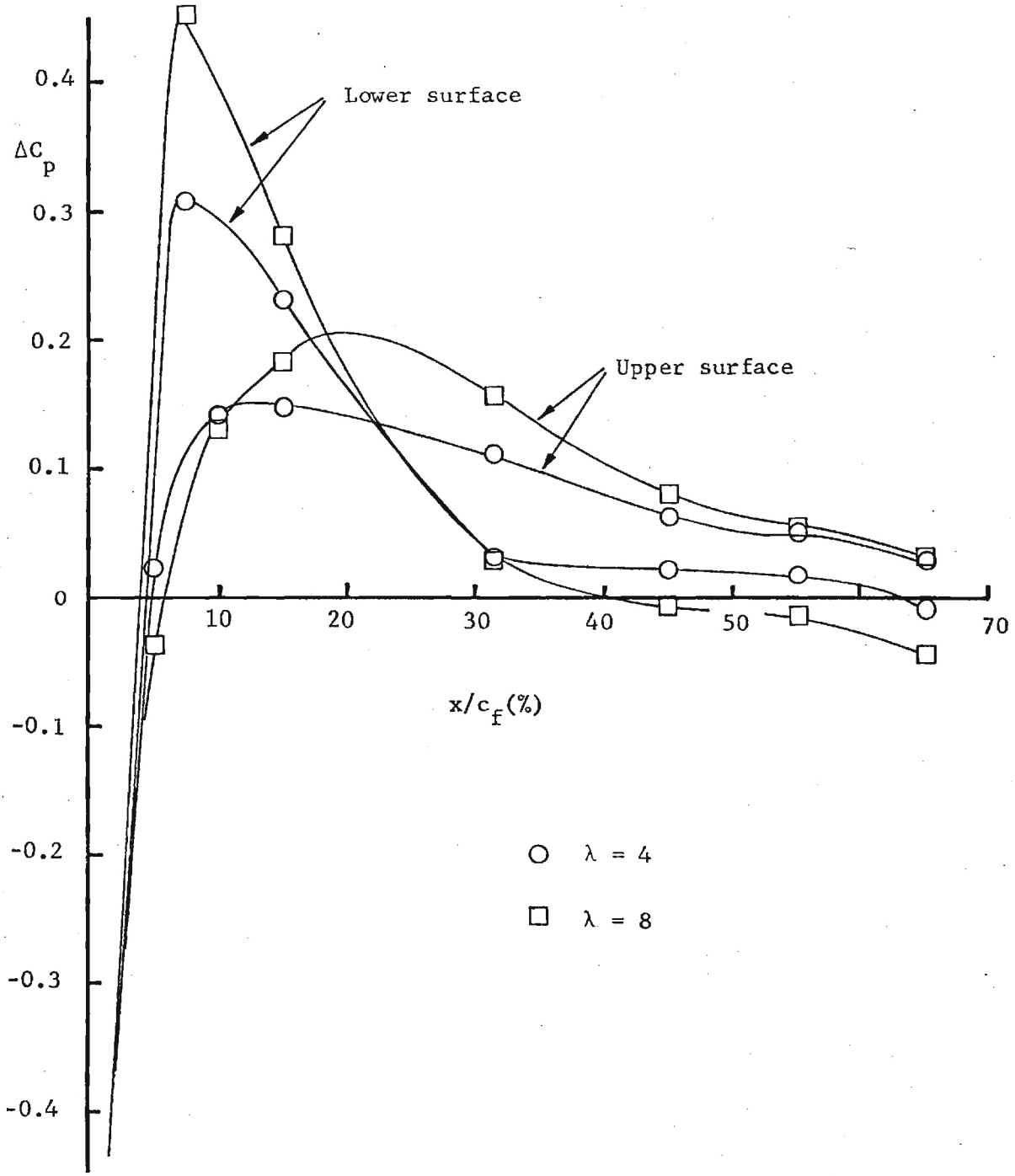

(a) $\alpha = 0^\circ$, $\delta = -5^\circ$ ($C_L = 0.034$)

Figure 19. - Variation of interference pressure distribution on flap with jet velocity. Y = 0.

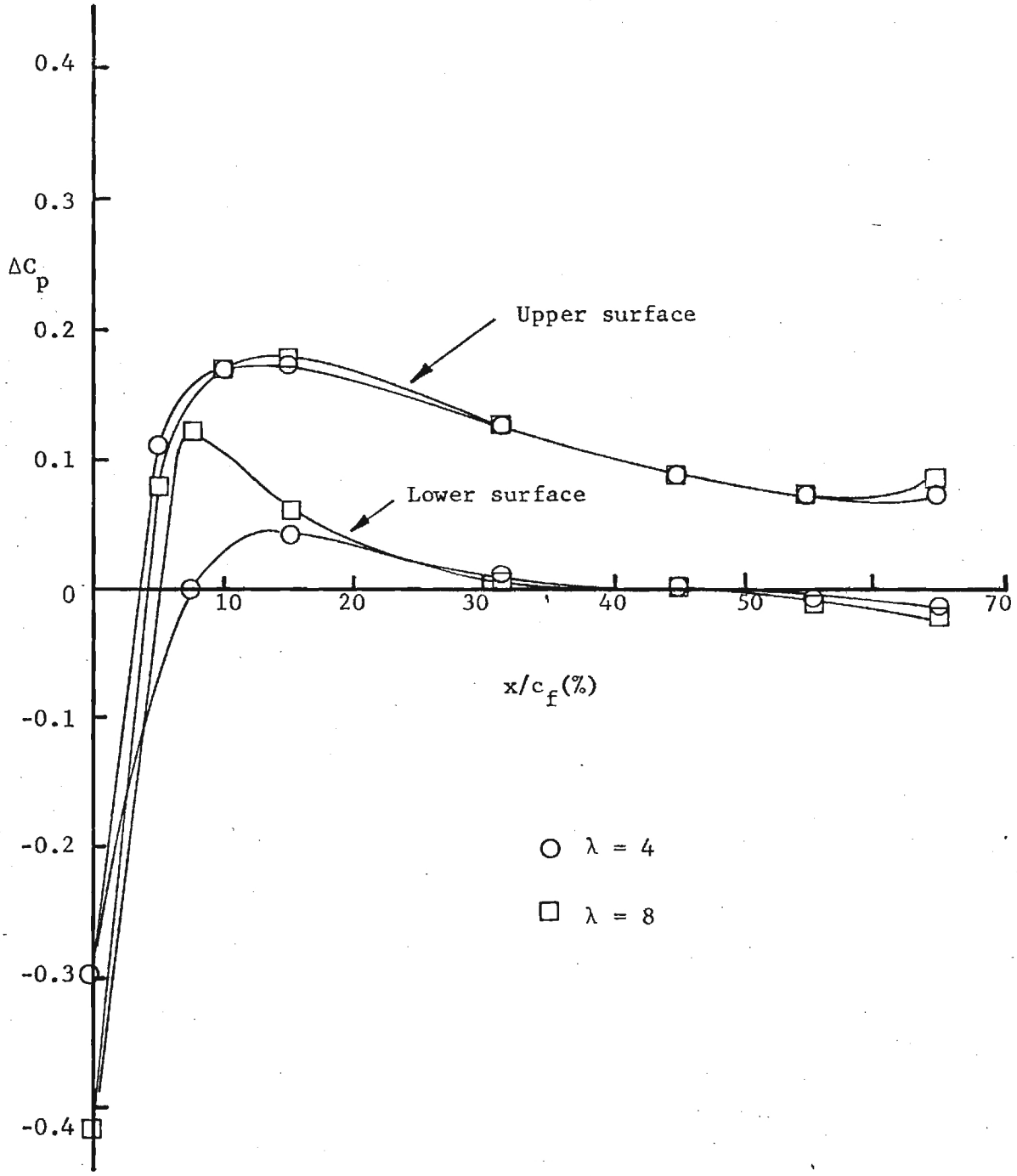

(b) $\alpha = 6^\circ$, $\delta = 0^\circ$ ($C_L = 1.24$)

Figure 19. - Continued

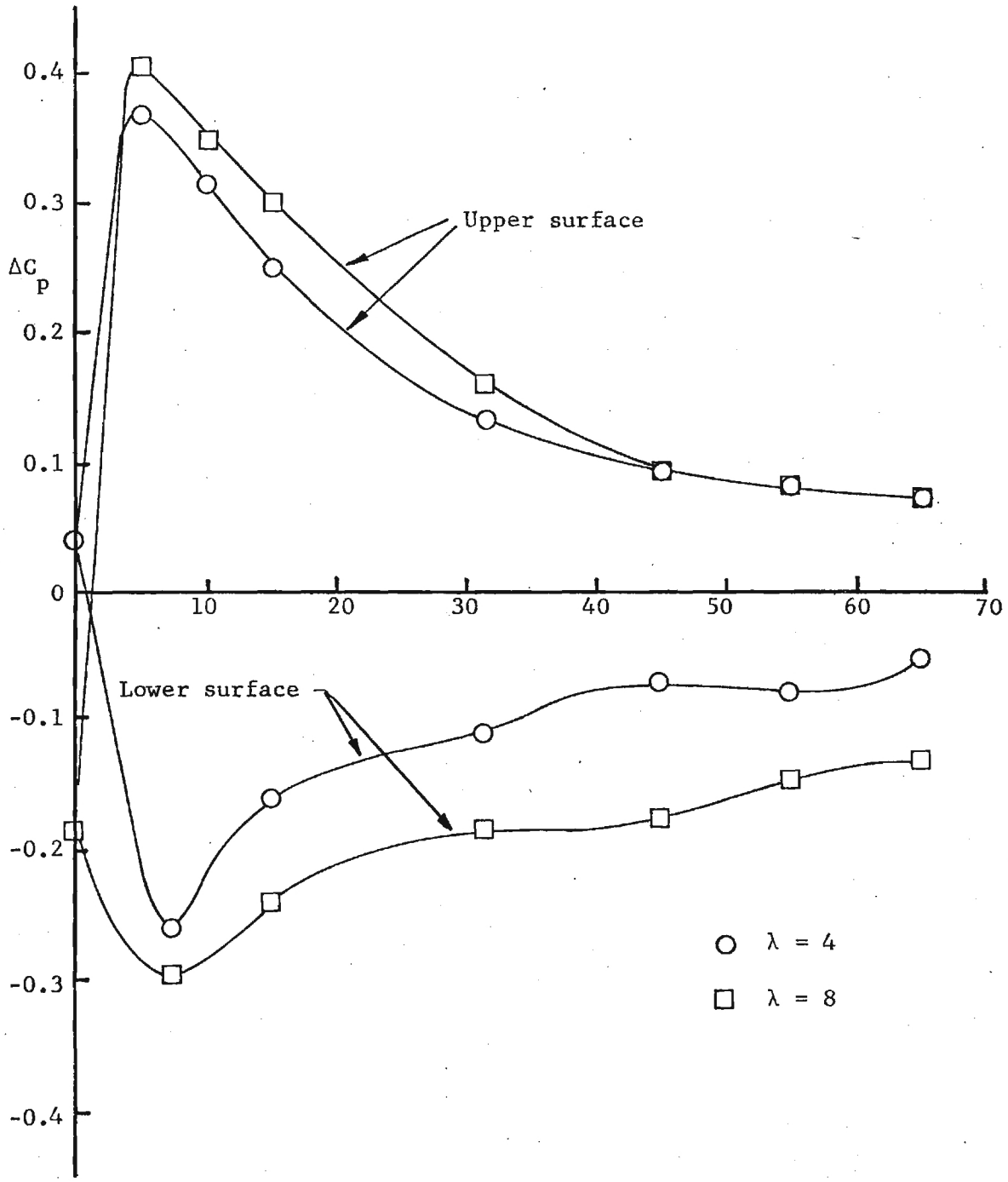

(c) $\alpha = 8^\circ$, $\delta = 15^\circ$ ($C_L = 2.45$)

Figure 19. - Concluded.

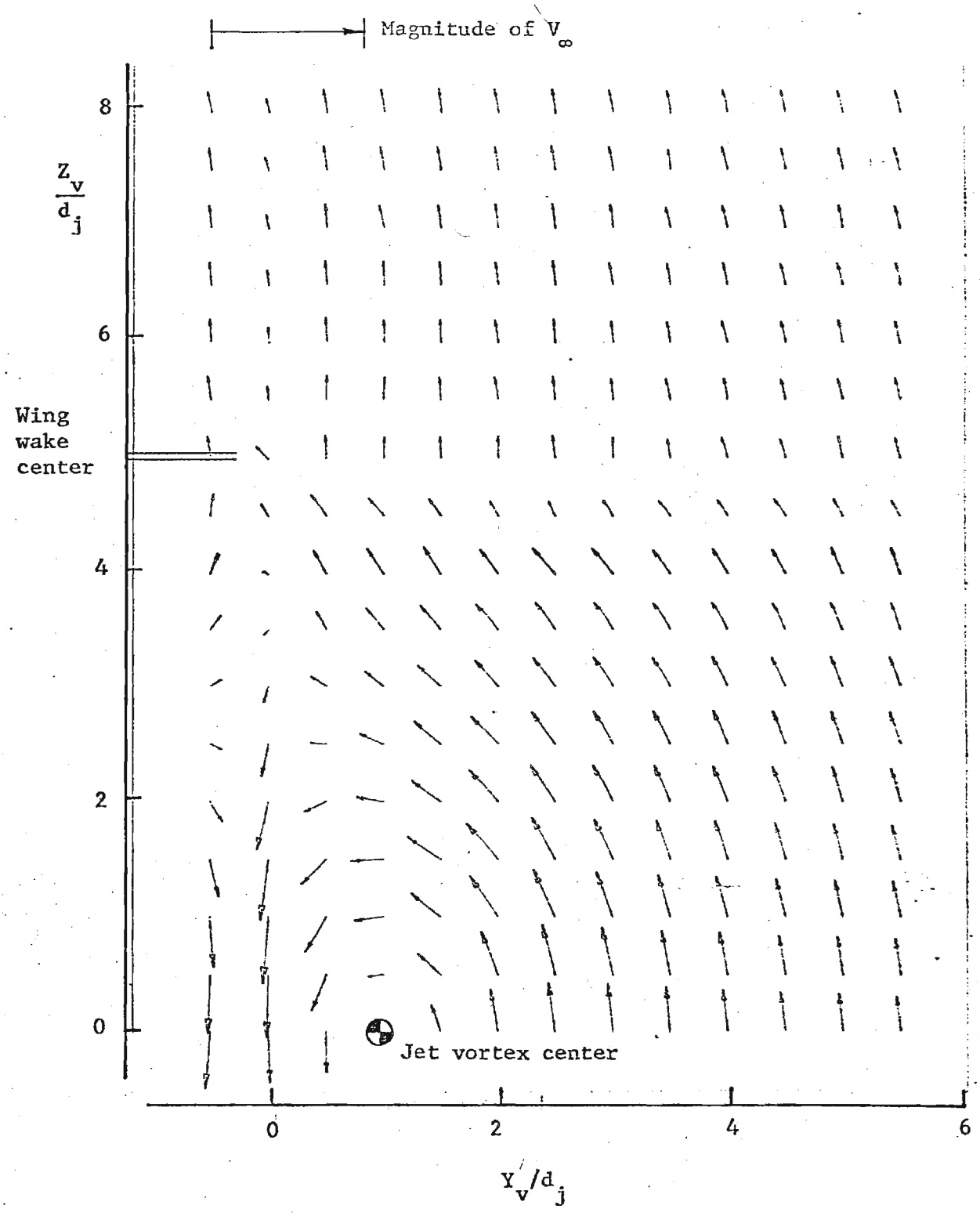

Figure 20. - Typical velocity vectors in Y_v-Z_v plane.
$C_L = 0.034$, $\lambda = 4$, $X/d_j = 8$.

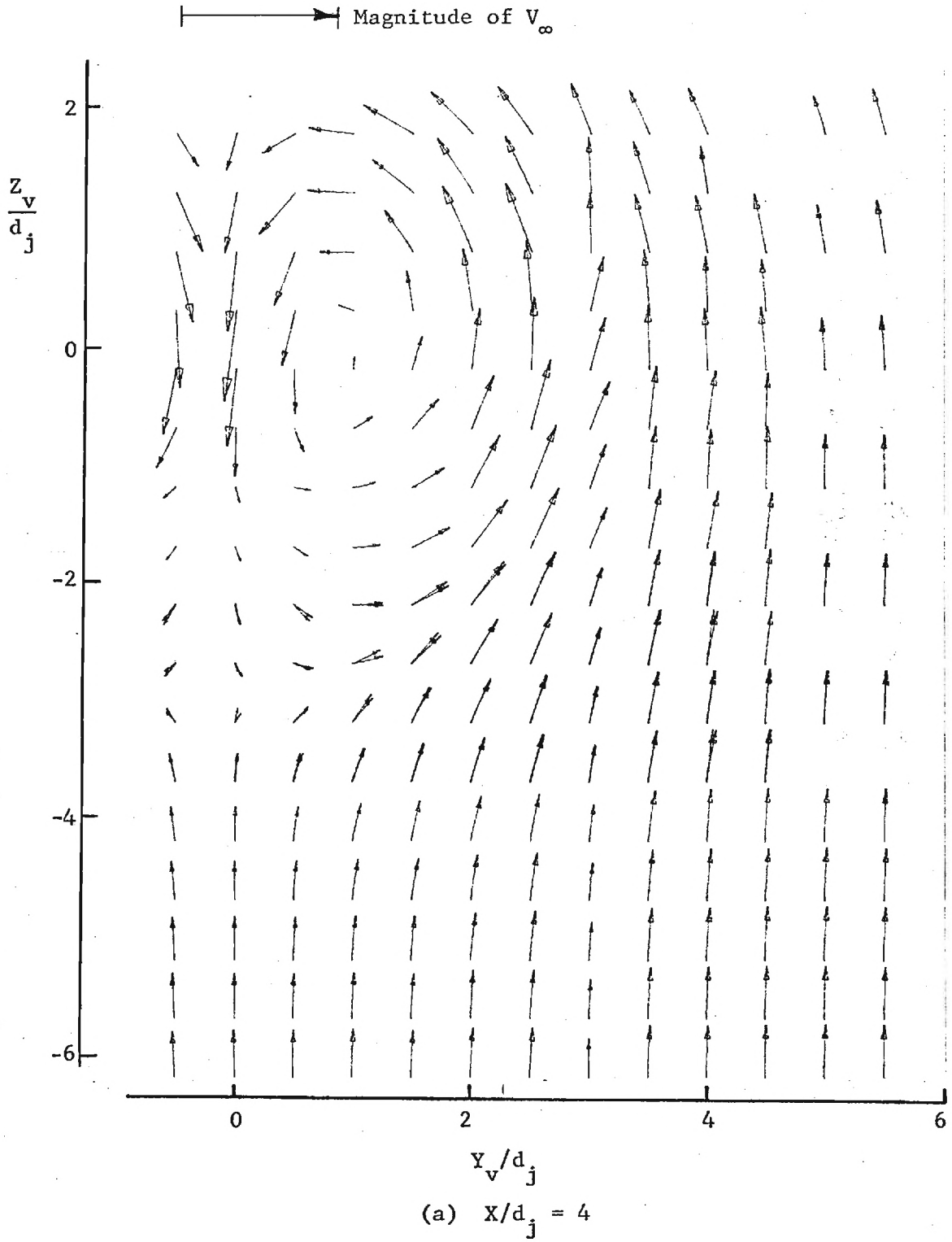

(a) $X/d_j = 4$

Figure 21. - Typical variation of velocity vectors in Y_v-Z_v plane with X/d_j. Lift coefficient 2.45, $\lambda = 4$.

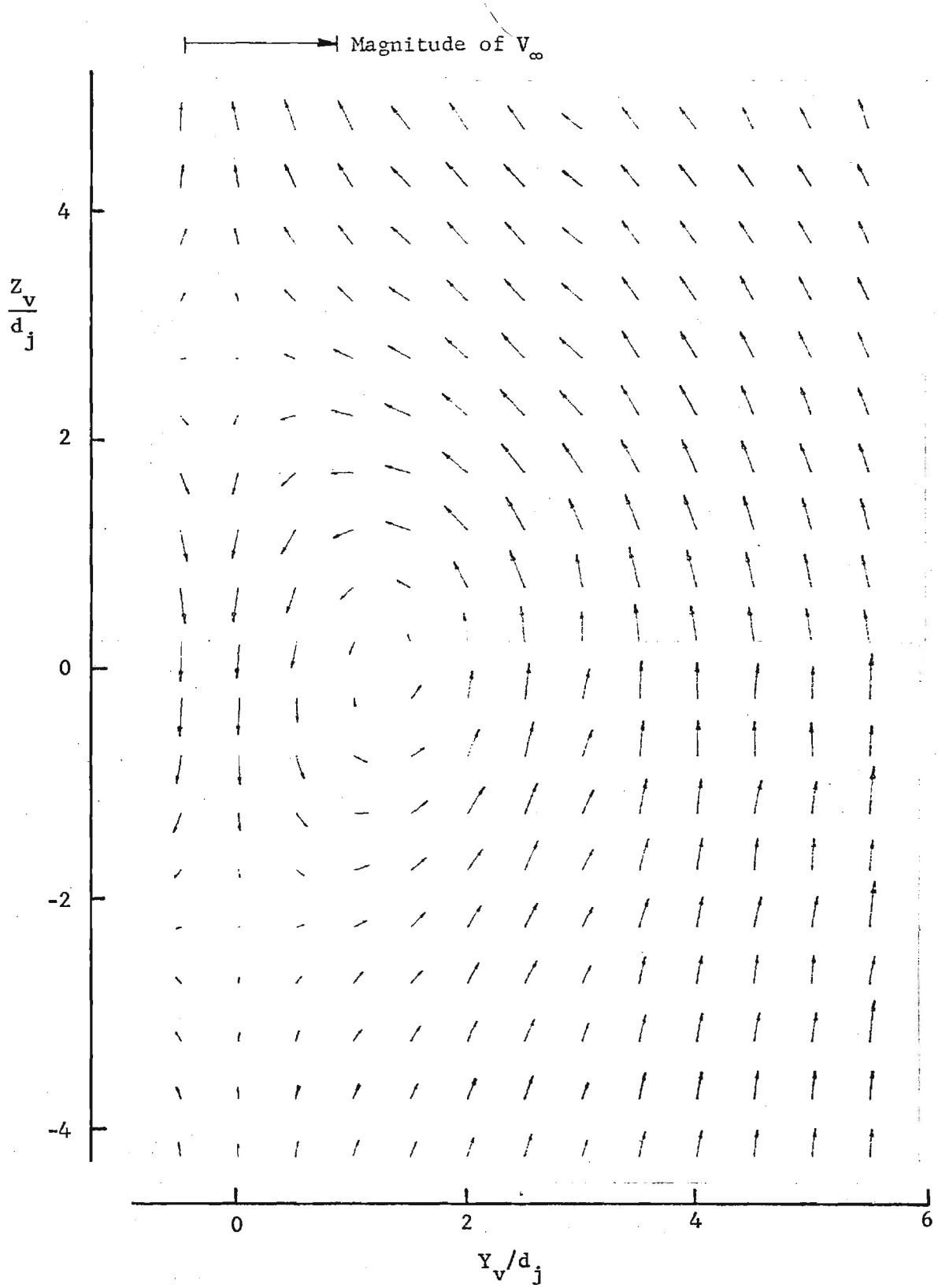

(b) $X/d_j = 14$

Figure 21. - Concluded

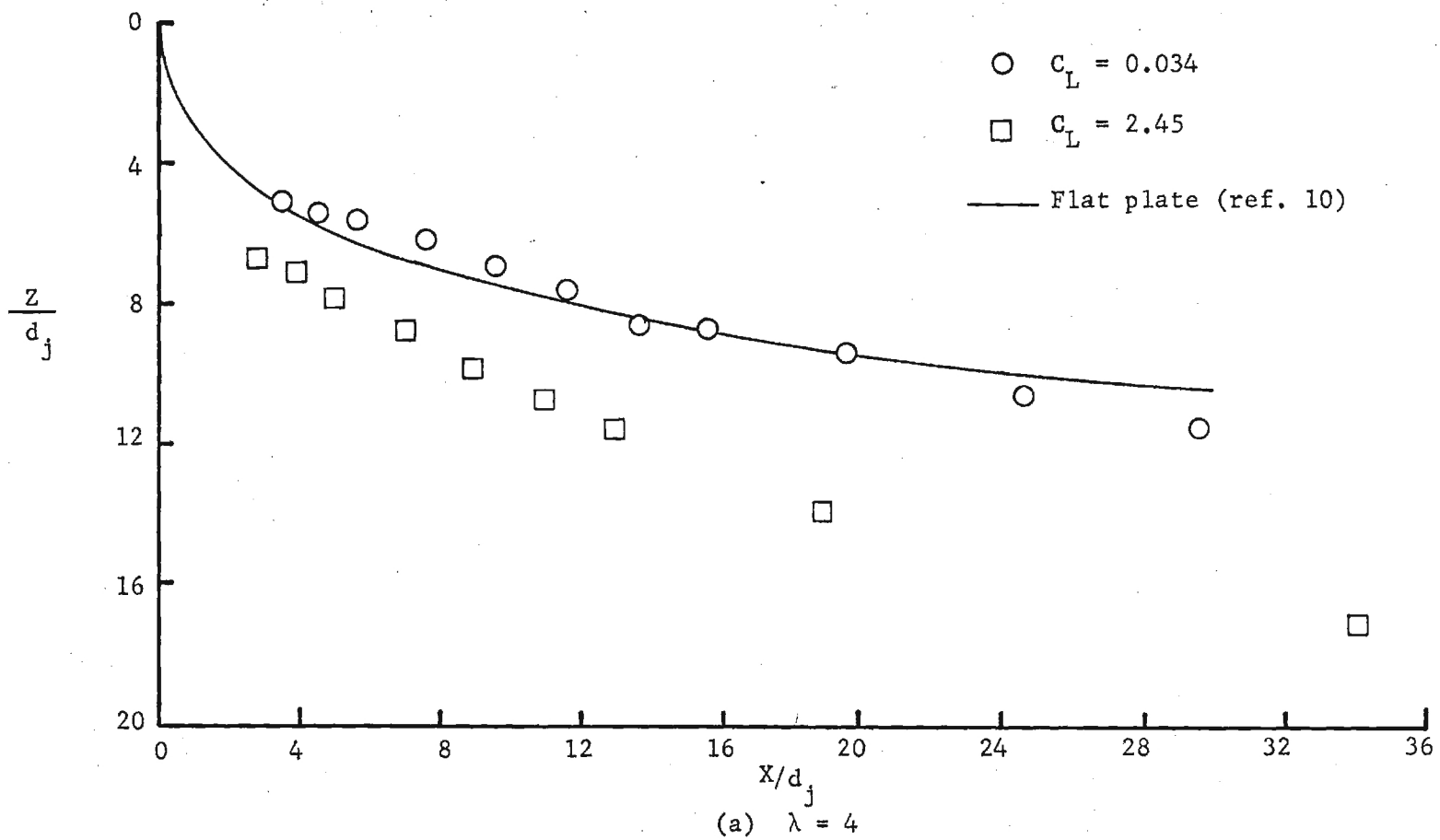

(a) $\lambda = 4$

Figure 22. - Variation of jet centerline with lift coefficient

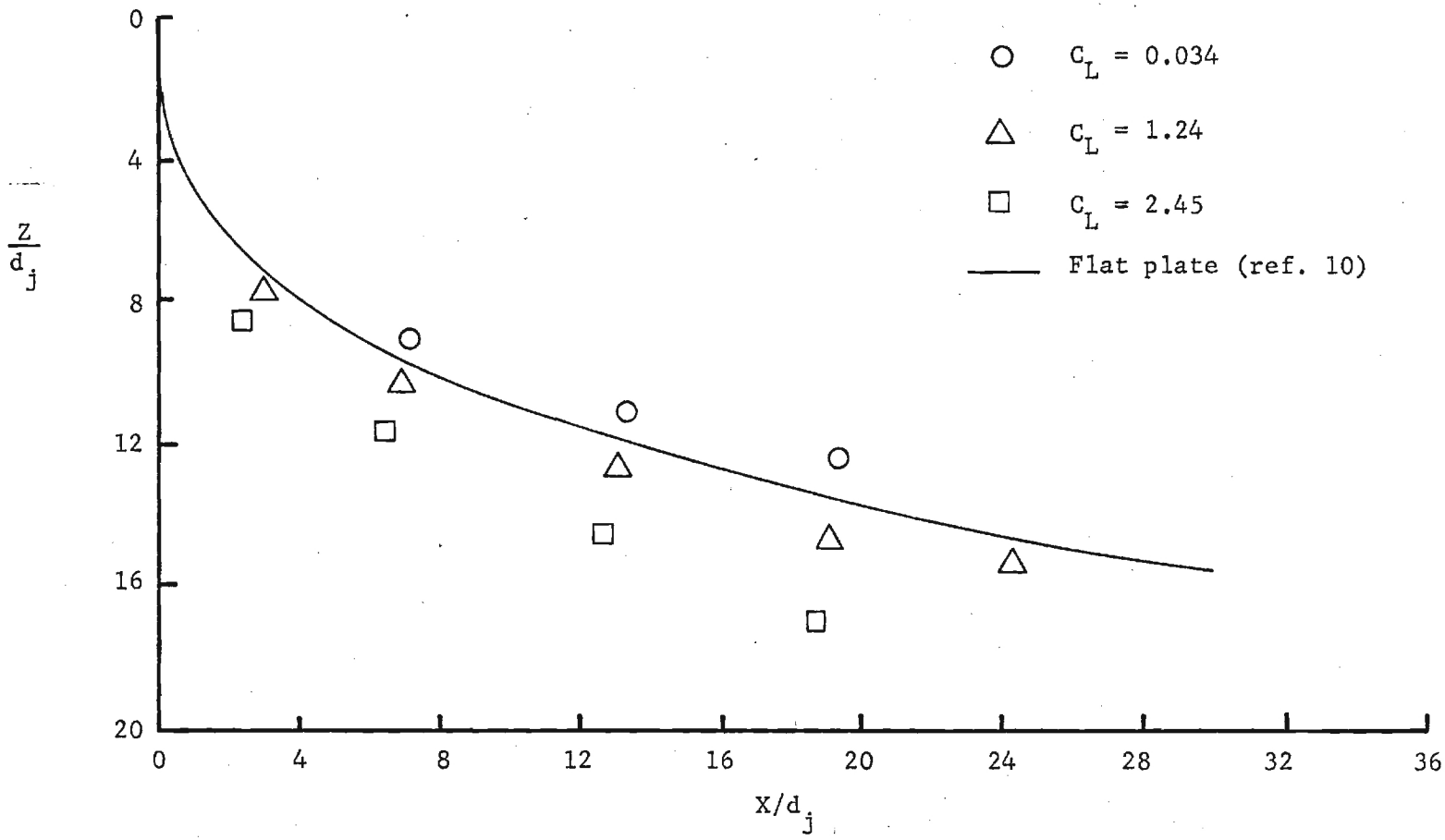

(b) $\lambda = 6$

Figure 22. - Continued.

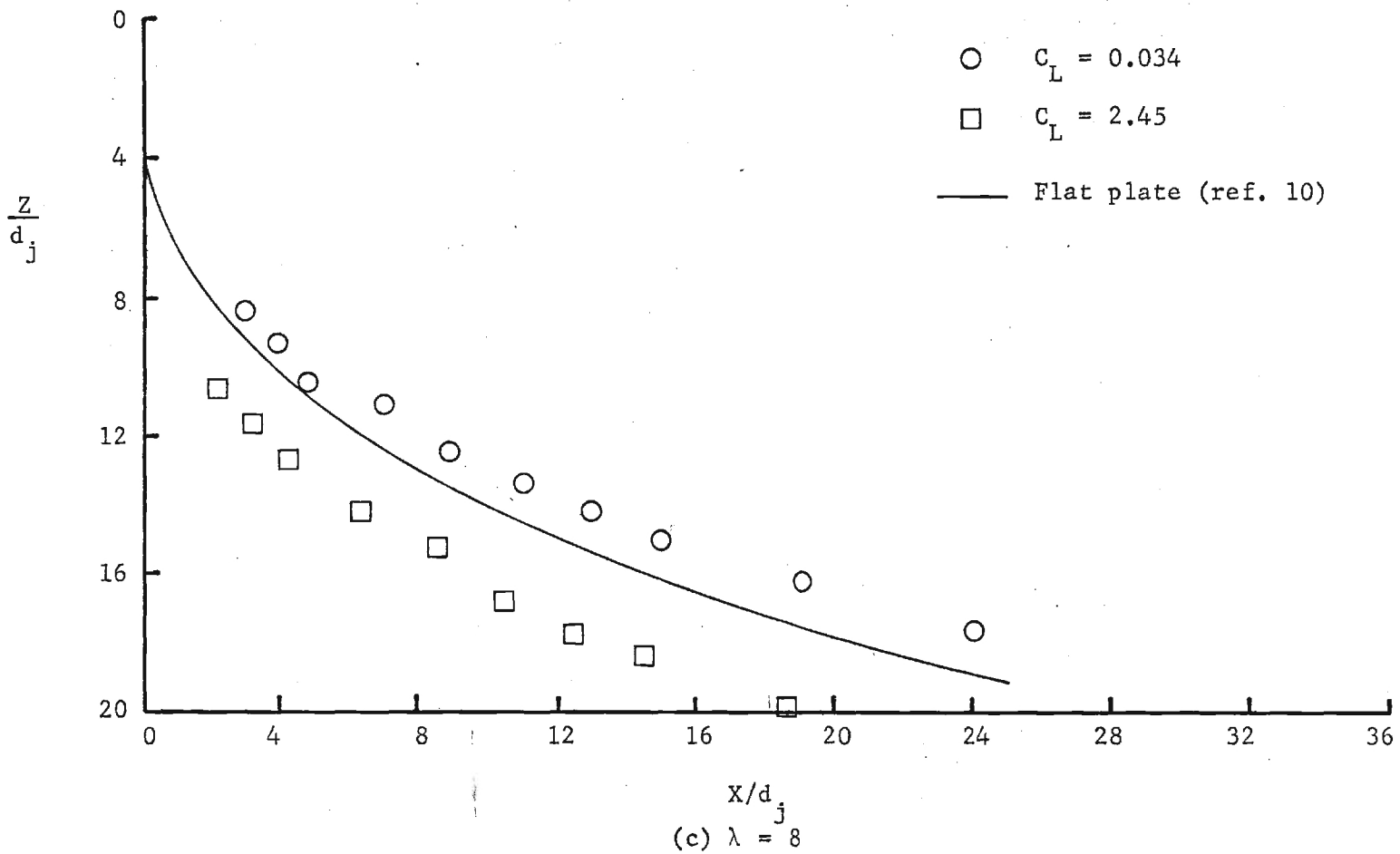

(c) $\lambda = 8$

Figure 22. - Concluded

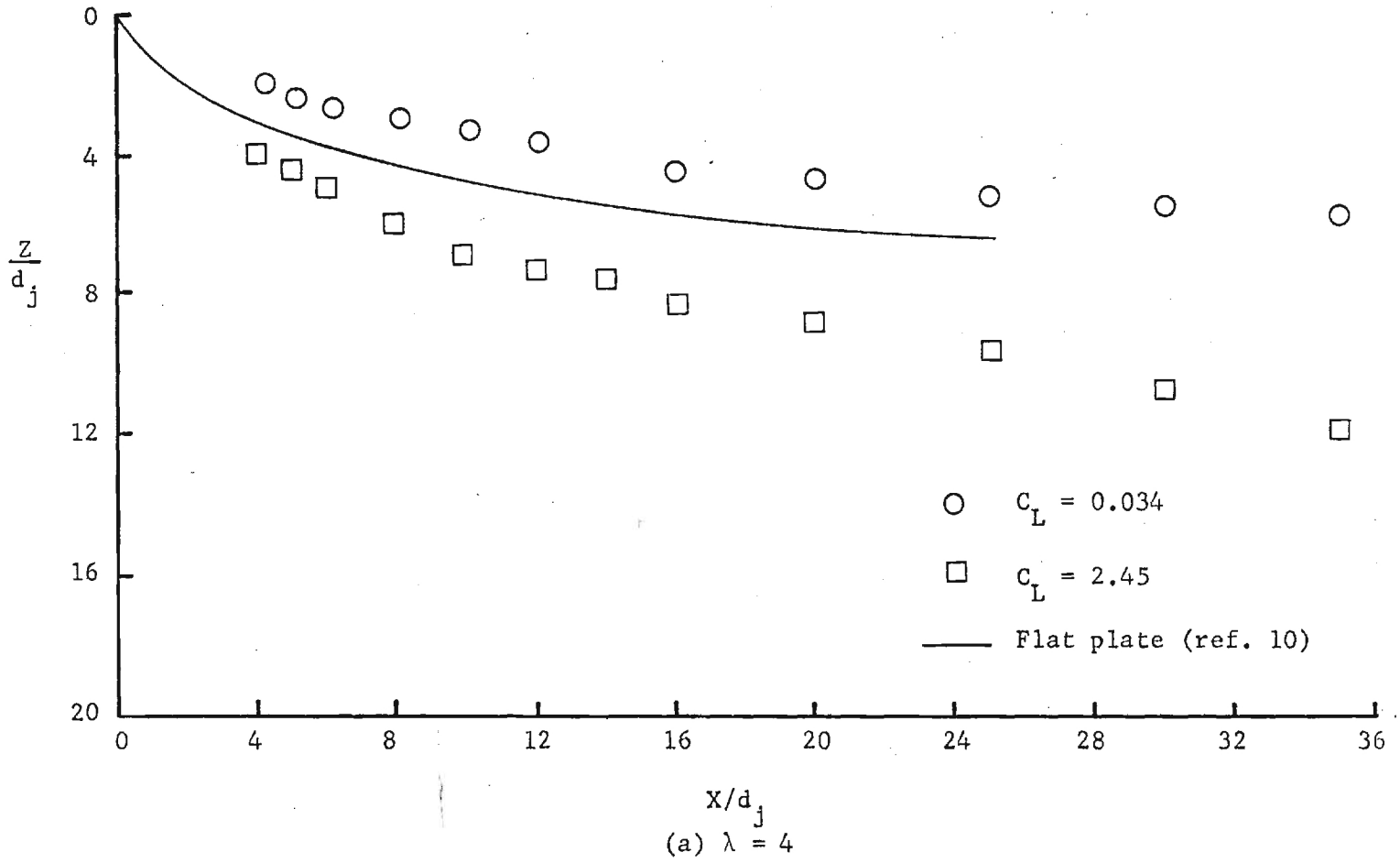

(a) $\lambda = 4$

Figure 23.- Variation of vortex curve with lift coefficient.

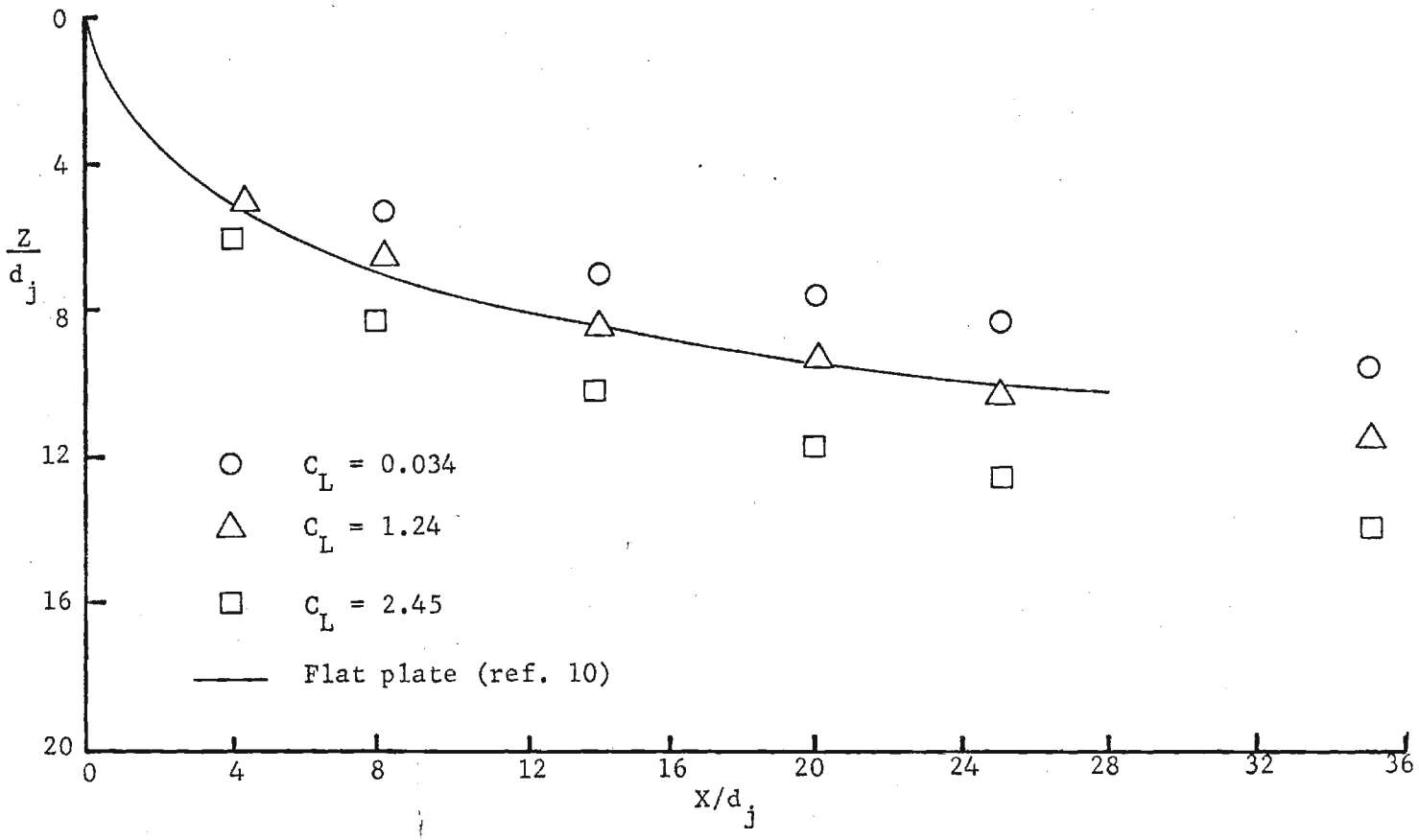

(b) $\lambda = 6$

Figure 23. - Continued.

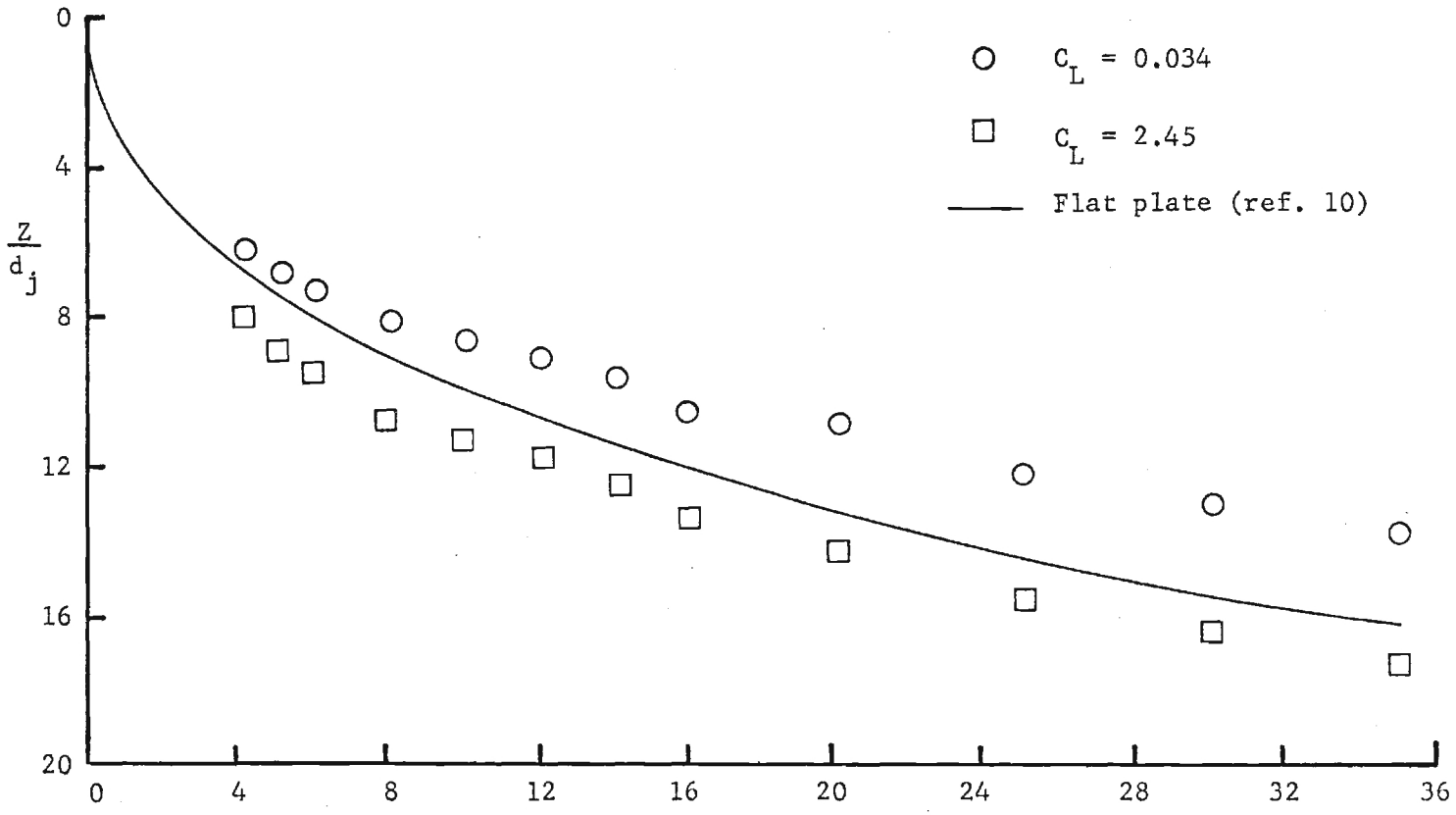

(c) $\lambda = 8$

Figure 23. - Concluded.

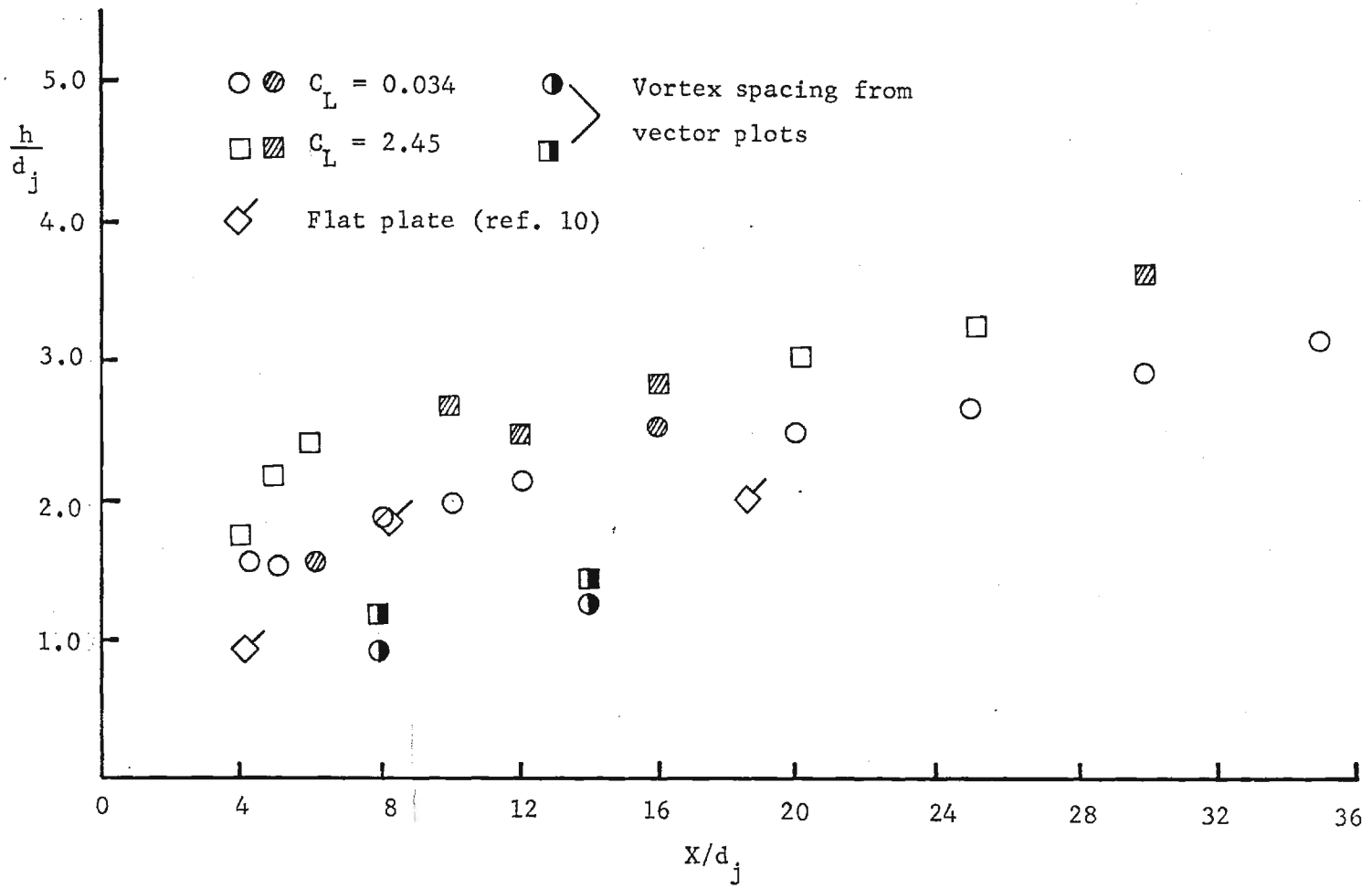

(a) $\lambda = 4$

Figure 24. - Variation of vortex spacing with lift coefficient.

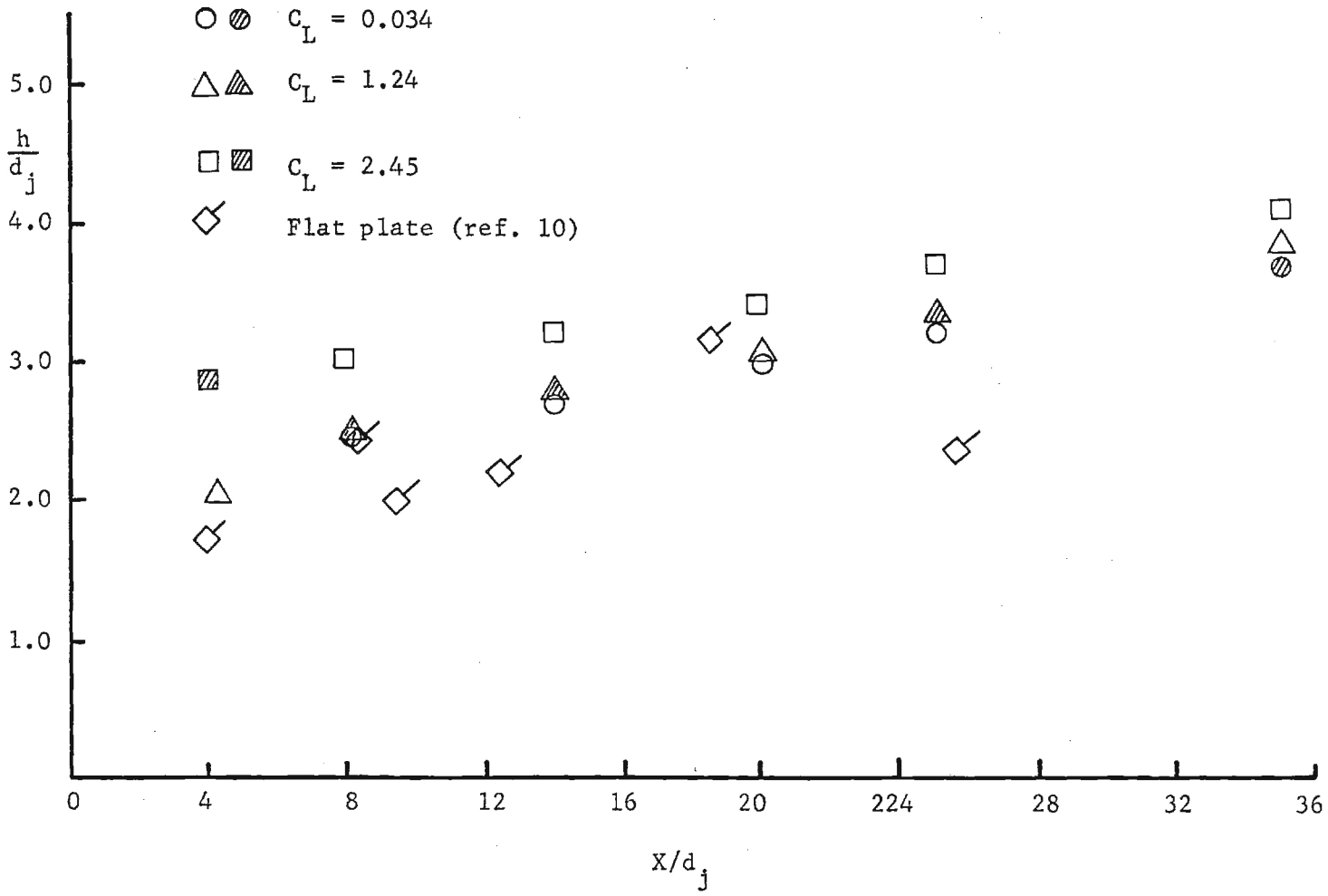

(b) $\lambda = 6$

Figure 24. - Continued.

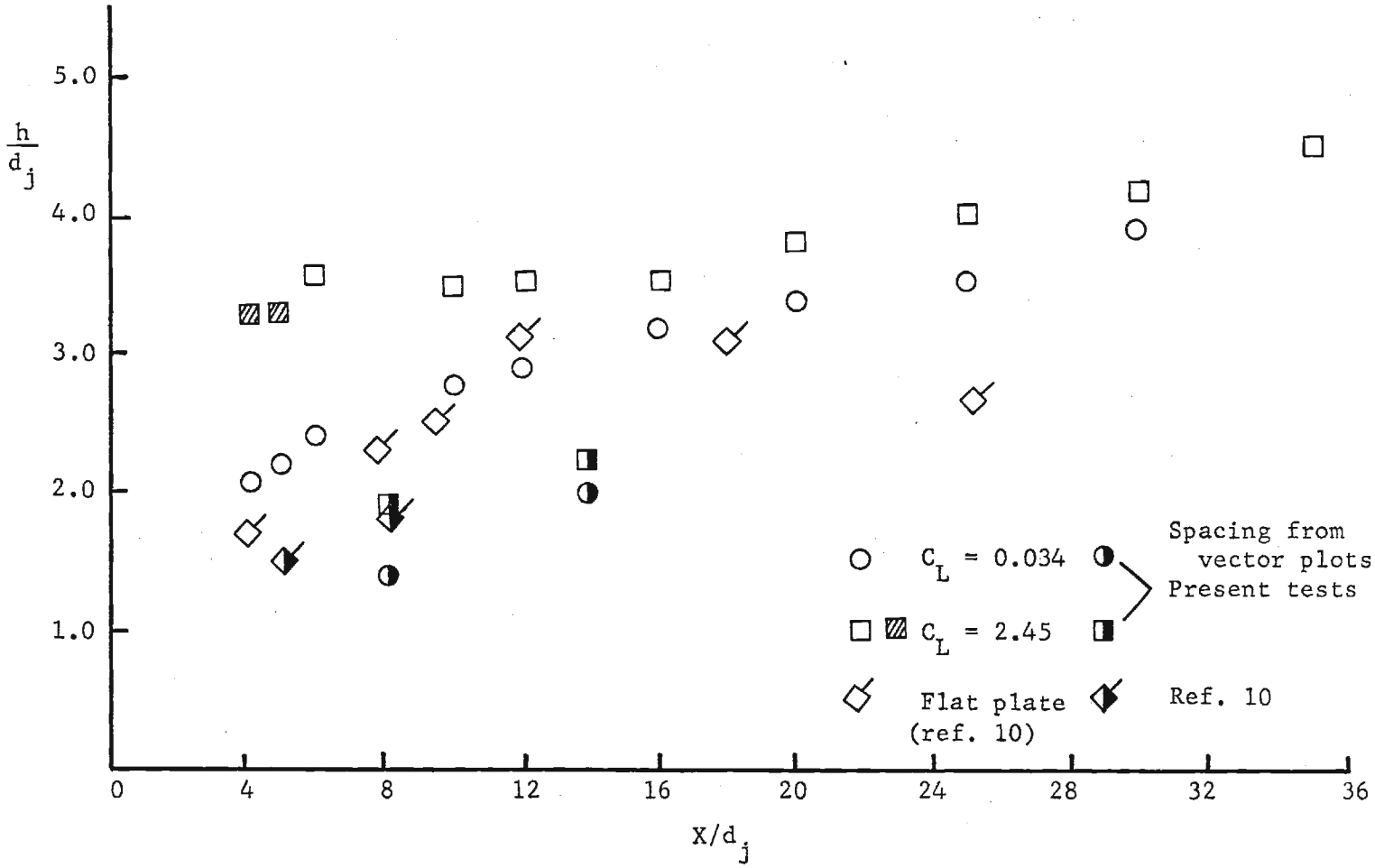

(c) $\lambda = 8$

Figure 24. - Concluded.

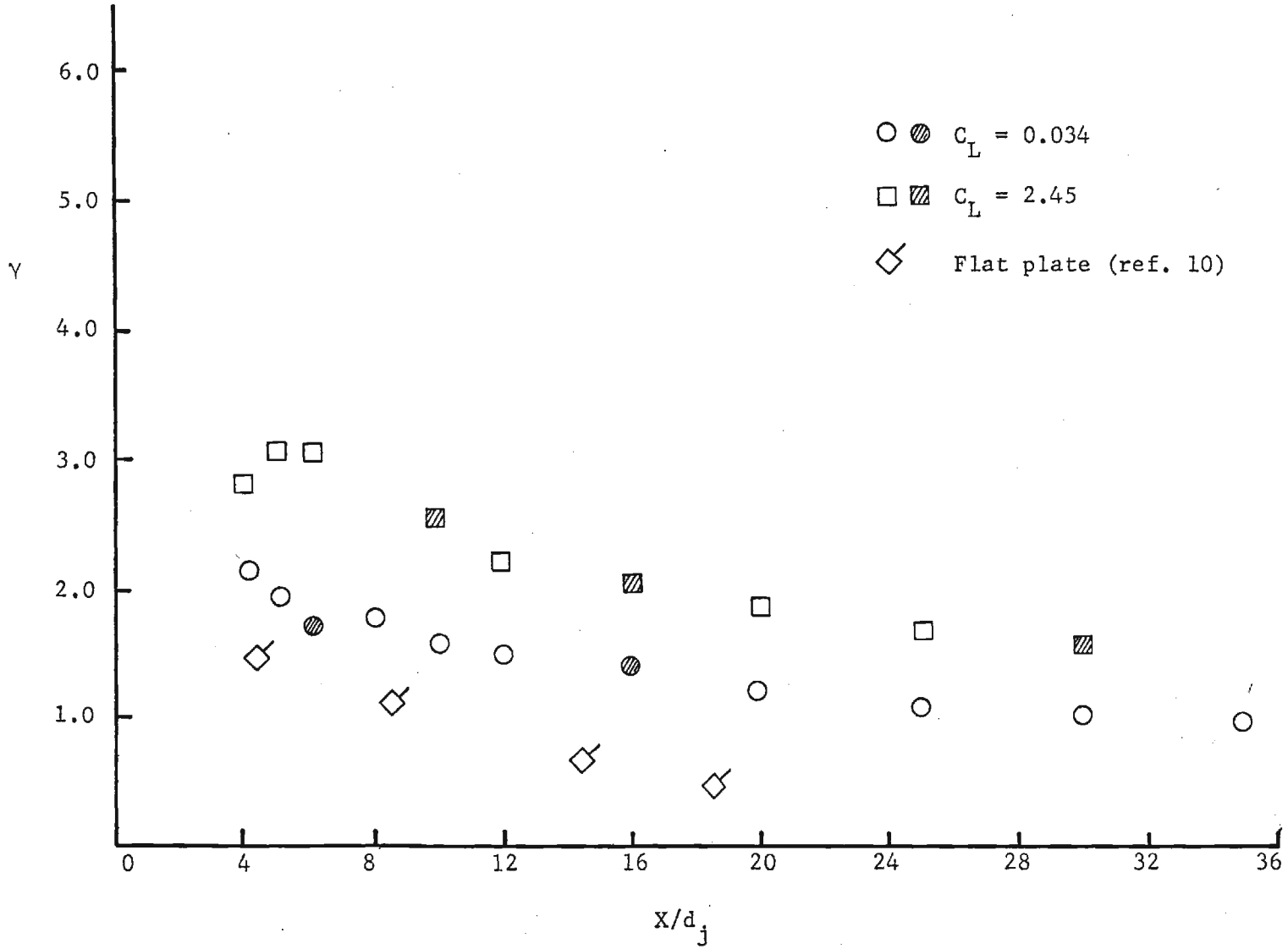

(a) $\lambda = 4$

Figure 25. - Variation of vortex strength with lift coefficient.

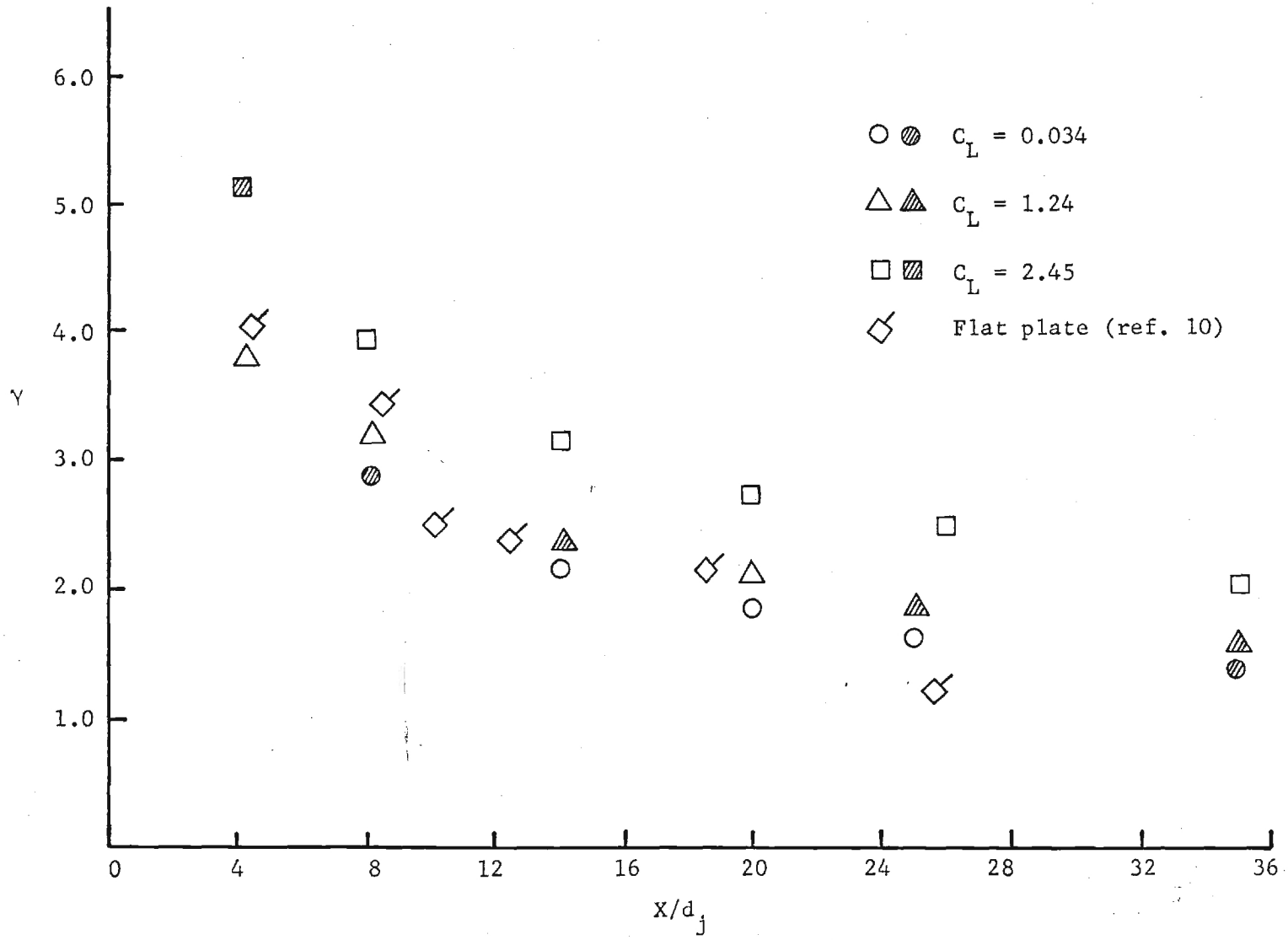

(b) $\lambda = 6$

Figure 25. - Continued.

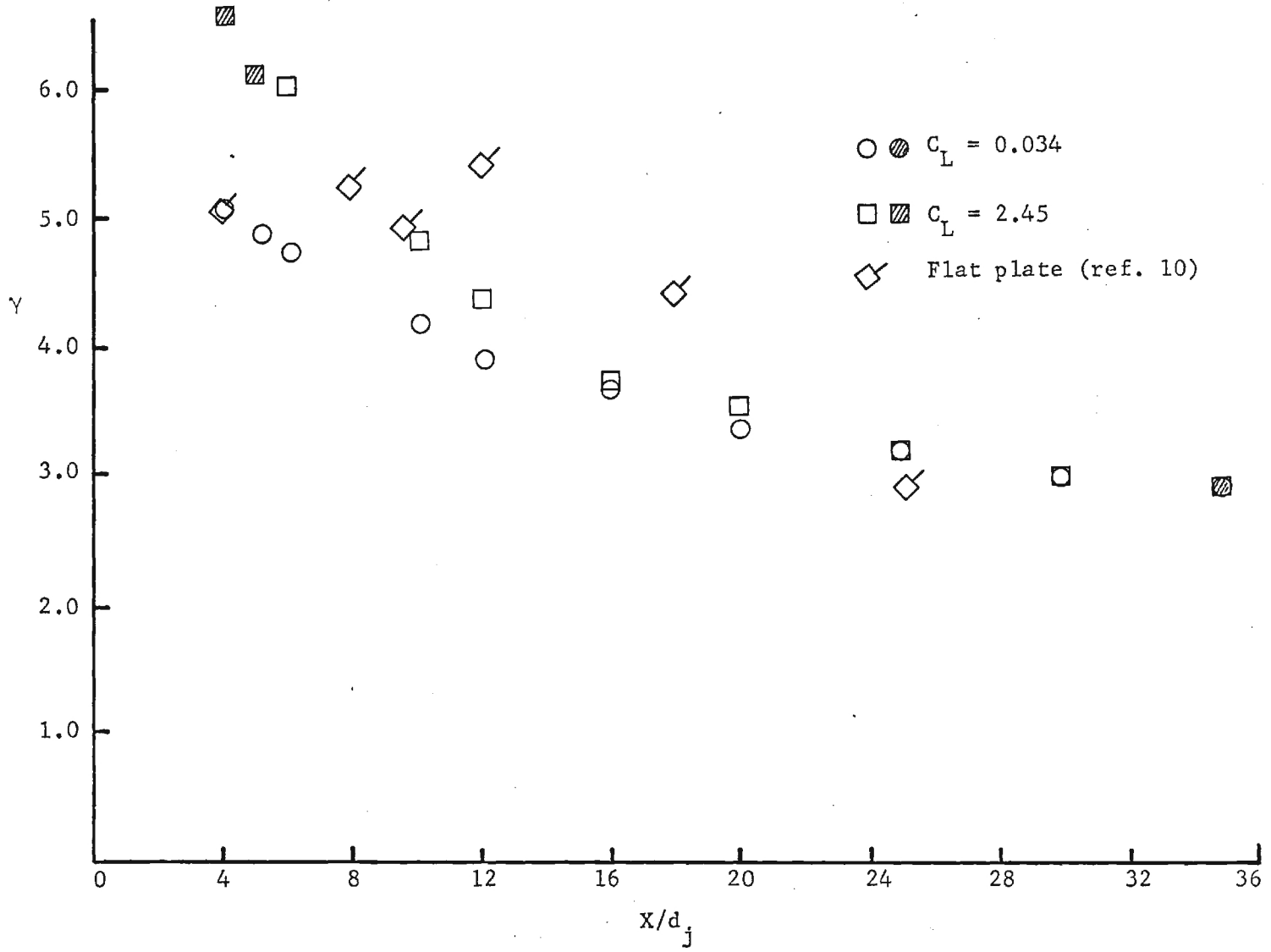

(c) $\lambda = 8$

Figure 25.- Concluded.